CORNEAL MATERIAL PROPERTIES AS A RISK FACTOR FOR POST-LASIK ECTASIA

Thesis submitted in accordance with the requirements of the University of Liverpool for the degree of Master of Philosophy by

Bernardo Teixeira Lopes

JANUARY 2019

TABLE OF CONTENTS

LIST OF FIGURES

LIST OF TABLES

LIST OF ABBREVIATIONS

3D	Three-Dimensional
AD	Ablation Depth
C3D15H	15-Node Solid Hybrid Elements
CCT	Central Corneal Thickness
DCT	Dynamic Contour Tonometer
FE	Finite Element
FEM	Finite Element Model
FT	Flap Thickness
IOP	Intraocular Pressure
LASIK	Laser Assisted in Situ Keratomileusis
MSE	Mean Spherical Equivalent
MPC	Multi-Point Constraints
Na+/K+-ATP	Sodium-Potassium pump
OCT	Optical Coherence Tomography
ORA	Ocular Response Analyzer
OZ	Optical Zone
PCT	Peripheral Corneal Thickness
PRK	Photorefractive Keratectomy
RPb	Refractive Power of back surface
RPf	Refractive Power of front surface
SMILE	Small-Incision Lenticule Extraction

ABSTRACT

Introduction/purpose: Myopic laser vision correction surgery, in particular Laser-Assisted in situ Keratomileusis (LASIK), is a common and widespread procedure in which tissue is ablated from the central part of the cornea. The resulting flattening decreases the corneal refractive power and allows the formation of sharp images at retinal plane in myopic eyes. Although it is a generally safe procedure, a complication related to an excessive reduction in the overall corneal stiffness, leading to visual impairment, has been reported as a major concern. Preoperative screening in order to exclude patients at risk to develop this complication is paramount. Several parameters have been described as relevant to preoperative screening. However, the corneal material properties so far have not been evaluated to this purpose. In this thesis, the corneal material properties were evaluated as a risk factor for post-LASIK ectasia.

Methods: Data from 32 eyes of 32 patients who have remained stable after LASIK surgery for correction of myopia and data from 4 eyes of 2 patients that developed post-LASIK ectasia including corneal topography, axial length, intraocular pressure (IOP) and surgery details were evaluated. Corneal topography, axial length and IOP were used to create eye-specific corneal models. A series of numerical simulations considering patient-specific models and actual surgical parameters with different corneal material constants was conducted. Error calculations between each numerically and clinically obtained corneal curvatures were used to estimate patient-specific corneal stiffness. The corneal material properties of both groups were compared. Normalised corneal material constants were used as previously described, with one being representative of the average normal population and a range between 0.5 and 2.5 representative of the physiological corneal stiffness.

Results: The average corneal material parameters on the stable group was 1.2 ± 0.6, and the average of the group that developed ectasia was 0.3 ± 0.2. There was minimum overlap between the groups.

Conclusion: It was observed that the patients that developed the post-LASIK ectasia presented considerably softer corneas compared to the patient that remained stable. To the best of our knowledge this was the first study to address this concept with a structured methodology and observe that the corneal material properties can be used as risk factors to the development of post-LASIK corneal ectasia during the preoperative screening to avoid the complication.

PREFACE

Sight is possibly our most important sense. The development of systems with the ability to perceive light had conferred to our most primitive ancestors, over millions of years, several evolutionary advantages. The ability to control a circadian rhythm, to identify the source light direction and final development of a high-resolution visual system, made possible the detection and pursuit of other animals, camouflage, and adornment to attract mates. In other words, sight enhanced our ability to interact with the world and with other beings (1).

The human visual system is a complex network, in which the eyes work as sensors capturing and transforming the light signal in the electrochemical stimulus conducted through the optic pathway until the visual cortex to allow image interpretation. In order to trigger this chain reaction, it is necessary that the light stimulus reaches the retina. This involves refracting the light by the eye optical system, the main structures of which are the cornea, responsible for around 70% of the refractive power of the eye, and the lens. If the ocular dimensions are not matched to the ocular refractive ability a blurred image will be formed on the retinal plane. To this inability of forming sharp retinal images is given the name of refractive errors.

The common refractive errors are usually classified as myopia, hyperopia and astigmatism. In the first two, the light refracted pattern is symmetric but not focused on the retinal plane, it is either before (myopia) or after it (hyperopia). Whilst in astigmatism the pattern is asymmetric and a single focusing point is not possible.

Myopia is the most prevalent refractive error around the world. It is estimated that by 2050, 5 billion people will be affected by it (2). The uncorrected refractive errors are one of the leading causes of vision impairment and the economic burden associated mostly with myopia, is more than 200 billion international dollars (3-6).

The correction of myopia can be achieved with the use of glasses, contact lenses or refractive surgery. Some authors addressed the quality of life issues of myopic patients. Shams et al, found that the quality of life of myopic patients is higher among the ones that underwent refractive surgery (7). Price et al observed that the easiness of night driving and overall satisfaction were higher among patients that were operated on than among contact lens or spectacle wearers (8). Rose et al, noticed that the impairment in quality of life of patients with high myopia was similar to those with keratoconus and more than 90% of patients with all degrees of myopia were aware of the possibility of surgical treatment and up to 60% of those were considering to undergo the procedure (9).

There are some refractive procedures currently available to correct myopia. Surgery can be undertaken on the corneal plane, by reshaping it so its focal length matches the retinal plane. This corneal reshaping can be achieved with the use of laser tissue ablation or with the implant of ring segments on the corneal stroma. Other surgical options are at the lens level. An auxiliary lens can be implanted either in the anterior or in the posterior chamber, or the replacement of a patient's original lens with a pseudophakic one can be performed. Even though there are many options, the most commonly performed, safe and with the highest degree of satisfaction procedure for myopia is the laser tissue ablation (10).

The foundations of corneal refractive surgery were laid around 70 years ago by the Spanish ophthalmologist José Ignacio Barraquer. In his *law of thickness*, he found out that the cornea flattens if you remove tissue from the centre or add it to the periphery, and conversely, it steepens if you add tissue to the centre or remove it from the periphery (11). Until the 1980's corneal reshaping was obtained by mechanical removal of the tissue with scalpels. The discovery of the excimer laser, which was able to disrupt biological tissue at a molecular level with minimum damage of the surrounding tissue, made possible precise and clean corneal reshaping, even with an observed increase in corneal temperature (12-14). So, in order to correct myopia, corneal flattening is obtained with precise laser tissue ablation.

The procedure's safety and effectiveness have been widely reported (8, 15). However, post-surgical ectasia is a major threat, and surgery must be avoided in patients at risk of developing it. In this complication, the cornea is softened beyond a threshold in which it can maintain its shape under the pressures that act inside and outside the eye, leading to progressive vision impairment and in extreme cases to the need for corneal graft surgery (16). Current screening methods are based on the identification of corneal shape patterns that could represent corneal fragility. This method is still fallible and ectasia has been reported in cases with considered normal shape, even in surgeries that promoted mild changes to the corneal tissue (17).

The amount of corneal flattening is related to the amount of tissue that is removed, wound healing and biomechanical responses to the surgery (18). It was observed clinically that patients undergoing higher amounts of myopia correction (resulting in a softer cornea in the postoperative) tend to present undercorrection (19, 20). Also, it was observed that regression after surgery (re-steepening of the cornea) was related to lower corneal thickness at the preoperative and to lower residual stromal bed at the postoperative (21). Along with the first clinical observations, that corneal structure was intimately related to the final shape after the surgery, devices able to measure corneal biomechanics *in vivo* were developed. This made understanding of this corneal feature possible in refractive surgery screening and planning (22).

Precise modelling of corneal material properties and refractive surgery were achieved with corneal numerical simulations (23, 24). However, the role of corneal material properties in evaluating biomechanical fragility prior to shape alterations, and relating this to the corneal ectasia after the procedure, has not been performed yet. In light of this, this thesis aims to study the corneal material properties in more depth and evalute its role as a risk factor for post-LASIK ectasia.

In order to help the reader to follow this thesis, it is structured in 5 chapters.

First chapter provides an introduction and background contextualisation. The aim and objectives of the thesis to address existing gaps in current knowledge are outlined.

Second chapter reports on the numerical modelling of the surgery and the corneal shape changes following the procedure while considering the material properties of the cornea.

Third chapter reports on the clinically-observed corneal shape changes in stable and ectasia cases.

Forth chapter compares the numerical predictions with the clinically-observed corneal shape changes. The chapter highlights the main outcome of the study that is the difference found in corneal material properties in patients that remained stable and those that developed post-surgical ectasia.

Fifth chapter discusses the results in relation to previously published literature, states the limitations and future plans and concludes the study.

Chapter 1: Introduction and Literature Review

1.1 Introduction

The ocular optics, refractive errors and their surgical correction have been extensively debated in the literature. There is also a considerable amount of work in understanding the biomechanics of eye with emphasis on the cornea. For example, a search in PubMed for those terms returns more than 100,000 entries. This knowledge supported the conduct of numerical simulations of the eye and study of its behaviour under internal or external forces, in order to be able to precisely predict in a virtual environment the ocular response to medical procedures (23).

In this chapter, the literature on eye structures and optical properties is reviewed. The refractive errors and their surgical correction, especially LASIK (most performed refractive procedure around the world) are also evaluated based on findings of previous studies. This is followed by a review of earlier clinical and experimental studies relating ocular biomechanics to refractive surgery outcomes. Finally, ocular and refractive surgery numerical modelling along with the evaluation of corneal material properties is reviewed and its gaps and limitations are briefly discussed.

1.2 Eye Structure and Optics

In this section, the structure and optics of the eye are discussed. The corneal features are reviewed in depth since the cornea is the most important refractive surface of the eye and its structure is normally remodelled in refractive surgical procedures.

1.2.1 General Anatomy and Physiology of the Eye

The eye is a fluid-filled, pressurised, slightly asymmetrical sphere. Its average sagittal length is about 24 to 25 mm and its average transverse diameter is of 24mm. The resulting volume is of 6.5 mL. Three outer layers, three inner fluid chambers and the lens compose the eye (25).

The outer layers are divided into external, intermediate and internal. The external layer is mostly composed (five-sixths) by a white and opaque fibrous tissue, the sclera. A clear, transparent, highly

specialised tissue in the front part of the layer is responsible for the other sixth, the cornea. A transition zone between both areas is called the limbus. This layer has a dual function. It isolates the inner part of the eye from the outer environment, and so protects the eye from foreign particles and infectious microorganisms and bears the intraocular pressure (IOP). It also permits the sight by allowing the light to enter the eye through the transparent cornea (26).

The intermediate layer, also known as uvea, is composed of three distinct but continuous structures. The iris and the ciliary body form the anterior part and the choroid forms the posterior part of this layer. The iris regulates the amount of light that enters the eye by its adjustable aperture, the pupil. The ciliary body anchors and regulates the shape of the lens in the process of accommodation and produces one of the ocular fluids; the aqueous humour. The choroid is mainly a vascular structure that oxygenates, nourishes and eliminates the metabolic sub-products of the eye, especially from the avascular inner structure, the retina (27). It has also a dark pigment, melanin, which prevents unnecessary light reflection that would interfere with the process of image formation (28).

The inner layer or the neural layer is called retina. It is composed of multiple light sensors; the photoreceptors and neural cells, to allow the transformation of light into an electrochemical signal that can be transmitted through the nervous system and processed by the brain (29).

The three fluid chambers are the anterior chamber situated between the cornea and the iris, the posterior chamber situated between the iris and the lens and the vitreous chamber situated between the lens and the retina.

Both anterior and posterior chambers are filled with a watery fluid; the aqueous humour. It serves as a surrogate to blood to the avascular cornea and lens that in order to maintain its transparency cannot afford to have blood vessels. So, it has the function to nourish the anterior and posterior chamber structures, remove excretory products of metabolism and help to stabilise the eye structure. It is produced and drained constantly, its turnover rate is of 2.4 ± 0.6µl/min (30). Its flow path starts at the ciliary body, where it is produced, reaches the posterior chamber, and after passing through the pupil

it reaches the anterior chamber. It is drained to the episcleral vascular system by the trabecular meshwork, located at the anterior chamber angle, between the cornea and the anterior iris and by an alternate pathway at the uveal meshwork and anterior face of the ciliary muscle (31). If the equilibrium of production and drainage of the aqueous humour is disrupted, the eye may face an increase in its pressure, which is a major risk factor for the development of glaucoma (32). The IOP measurement by the applanation method is also highly influenced by the corneal thickness and the measurements in naturally thin or thinned corneas due to refractive surgery tend to be underestimated (33-35).

The vitreous chamber is filled by a gelatinous substance, also transparent; the vitreous humour. It accounts for most of the volume of the eye, around 80%. It is responsible for maintaining the eye's shape and the presence of phagocytic cells results in cleaning of blood cells and cellular debris that could interfere with light transmission. It also keeps the retina in place, by pushing it back towards the choroid (36).

The crystalline lens is a transparent biconvex structure responsible for refracting light. In order to keep its clarity, it has no blood vessels after foetal development. All its metabolic requirements and waste carry off is dependent on the aqueous humour (37). It lies between the iris and the vitreous humour and is suspended by thin strong fibres, the zonules of Zinn. They are attached to the crystalline equator and to the ciliary body (38). The contraction of the ciliary muscles and relaxation of the zonules affect the crystalline lens shape, making it more spherical, increasing its refractive power and favouring near vision. This process is known as accommodation (39).

The lens is constantly growing throughout the aging process. Meanwhile, it assumes an increasingly curved shape that can increase the refractive power of older lenses (40). Nevertheless, a myopic shift is not always observed in elderly patients because the refractive index reduces with age due to, among other factors, an increasing of water nuclear content and an increasing presence of insoluble protein particles (41). Therefore, either a myopic or a hyperopic shift can happen according to the balance between these two processes.

1.2.2 Anatomy and Physiology of the Cornea

The cornea is the frontmost outer part of ocular tissue. Along with its role in protecting and shaping the eye, it is together with the tear film in front of it the most important ocular refractive surface, responsible for approximately 70% of the total refractive power. It has a complex structure formed by several components carefully arranged in order to keep its transparency and geometrical shape. The study of corneal anatomy, physiology and biomechanics are of extreme importance in refractive surgery procedures.

Corneal Anatomy

The cornea has an almost circular cross-section with the horizontal diameter measuring from 11.5 to 12mm and the vertical diameter measuring 1mm less than that. Its thickness is thinner at the centre and gradually thickens towards the periphery. The shape of the cornea is prolate and aspheric with the centre being steeper than the periphery resulting in less spherical aberration (42). Corneal shape and curvature are a result of its intrinsic biomechanical properties under IOP and external forces affecting the eye (18). The organisation and distribution of the collagen bundles in the anterior stroma providing a higher stiffness to this region appear to be important to the maintenance of corneal shape and curvature (43).

Traditionally the human cornea has 5 distinguishable layers: epithelium, Bowman's layers, stroma, Descemet's membrane and endothelium. More recently a new layer, the Dua's layer, between the posterior stroma and the Descemet's membrane has been described with particular importance in corneal graft surgery (44). However, it was subjected to some criticism as to its existence and on its eponym (45, 46).

The cornea has a stratified squamous non-keratinised epithelium composed of 4 to 6 layers (47). Its thickness is approximately 50µm (48). The most superficial epithelial cells have projections to increase the surface of contact with the tear film and are firmly adhered to each other with tight junctional complexes. This inhibits tears from entering the intercellular space and works as a barrier to toxins

and microorganisms (26). There is a complete turnover of the cells in around 7 days (49). And its thickness is not uniformly distributed, which is important to the final optical effect of the eye smoothing some surface irregularities (50). This feature must be taken into account in laser refractive procedures since it can modify their effect (51). While it is important to the eye optics, the interaction with the tear film and the protection against external agents, corneal epithelium plays a small role in corneal biomechanics (52).

The Bowman's layer is an acellular, non-regenerating condensation of randomly distributed collagen fibres and extracellular matrix that is placed between the epithelium and stroma (53). Recently, its transplant is proposed to treat advanced stages of corneal ectatic disease (54).

The thickest layer of the cornea is the stroma that represents around 90% of the tissue. Its three primary non-aqueous components are collagens, proteoglycans and cells. The collagen fibres and the extracellular matrix are regularly disposed of, which is important for corneal transparency (55). The stroma is the most relevant layer in corneal biomechanics properties. The lamellar interweave and the 3D collagen structure, are important to explain the corneal biomechanical properties (56). Some other aspects also influence the biomechanics, such as the crimps of the collagen fibres, which are not straight on a micro scale (57).

The most prevalent cellular component of the stroma is the keratocytes. They are more prevalent in the anterior stroma and synthesise collagen molecules, glycosaminoglycans and matrix metalloproteases, which are all crucial in maintaining the extracellular matrix and the homeostasis of the tissue (58). Up to one-third of the cellular soluble protein content is composed of "crystalline", this protein reduces the light backscatter of the keratocyte and contributes to corneal transparency (59).

The basement membrane of the endothelium is the Descemet's membrane. It is a thin membrane, composed of two parts. The anterior part, 3µm thick, is secreted before birth and possesses a distinctive banded pattern. The posterior part is unbanded and secreted after birth. It thickens with

age and can reach 7µm in older adults (60). Its major components are collagen type IV, present in most basement membranes, and collagen type VIII, more specific to the Descemet's membrane, which is important to its correct assembly and corneal stability (61).

The corneal endothelium is a thin single layer that covers the Descemet's membrane and is in contact with the aqueous humour (62). It is highly metabolic, active with the Na^+/K^+-ATP pump and the intracellular carbonic anhydrase pathway, important to regulate the corneal hydration state and transparency (63). It also has a high number of Golgi complex resulting in high secretory activity responsible for the secretion of the Descemet's membrane (64).

1.2.3 The Optical System of the Eye

All these structural components previously described are arranged in order to obtain the best optical performance. The ocular optical system is the result of its two main refractive bodies, the cornea and the lens, the pupil and the retina.

The cornea is a meniscus lens. Its surface roughness at the outer epithelium is smoothed by the tear film to improve its optical quality (65). It has a toric-ellipsoid shape that works to compensate the optical spherical aberrations present in perfect spheres. This is not completely possible since the cornea is off-axis resulting in horizontal coma aberrations (66). However, the measured aberrations of the cornea are higher than those of the whole eye, and it has been demonstrated theoretically and clinically that the angle of incidence of the light in the cornea and its internal structures such as the young crystalline lens work to compensate these aberrations (67-69).

It is challenging to study the lens optics. Its shape and refractive power change considerably with accommodation and it keeps growing continuously with age (70). Another complexity factor present in the human lens is that its refractive index increases from the surface towards the centre, creating a gradient index (71). Apart from the aberrations that, as mentioned partially compensate the corneal aberrations, light scattering can affect the lens. The young lens is highly transparent and interferes minimally with light transmission. With ageing and pathological processes, the fibrous component of

the lens gradually increases light scattering and loss of transparency resulting in the formation of cataract (72).

The pupil is nasally dislocated about 0.5mm from the optical axis which may produce ocular aberrations, such as coma (73). However, it is a contractile diaphragm that controls the light entrance to the eye. With high light levels, the pupil contracts reducing the aperture size, this reduces the incidence of peripheral rays that are more aberrated than the central. In low light situations, it dilates to increase the number of photons entering the eye. Even receiving more light from the periphery with greater amounts of aberrations, to increase the number of photons entering the eye is important for a better signal-to-noise ratio. So the pupil can balance the noise and optical blur to obtain an optimal adjustment between factors that can affect optical quality (74).

The retina not only plays a role in converting the light signal to something that can be transmitted to the central nervous system and interpreted, but it also has optical functions. The curvature of the retina corresponds to the curvature of the image, which allows for a better peripheral resolution (75). Also, each cone, the most common photoreceptor cell of the macular centre, functions as an individual waveguide that points approximately to the centre of the pupil. In this way, the maximum image resolution will be obtained in the centre. The lower luminous efficiency of the peripheral rays diminishes their aberrations.

The optical components are relatively asymmetric and misaligned, resulting in an imperfect optical system. However, the eye is a robust optical system (76). These imperfections and misalignments are displayed in such a way they are able to compensate each other.

1.3 Corneal Surgery for Correction of Refractive Errors

It was discussed previously that the refractive errors can be corrected with glasses, contact lenses and surgery. The imperfect optical status (aberrations) of the eye was also considered. Regular glasses and

soft contact lenses are only able to correct the less complex aberrations of the eye or low order aberrations, while the surgery can act on more complex or high order aberrations. The low order aberrations comprised by myopia, hyperopia and astigmatism are more relevant for visual acuity reduction and as seen previously not all high order aberrations are bad (77). In addition to that, surgery can produce high order aberrations and their correction is often desirable for a significant number of patients (78).

As observed by Barraquer in his *law of thickness*, removing tissue from the centre of the cornea causes flattening and from the periphery causes steeping (11). Laser corneal surgery is the current gold-standard procedure to achieve this reshaping. The procedure is flexible and can be done in several ways. Tissue can be ablated from the corneal surface (photorefractive keratectomy – PRK) or below a corneal flap (LASIK) and it can also be removed in the form of a lenticular button without disrupting completely the above corneal tissue (small-incision lenticule extraction – SMILE).

The most performed surgical procedure is LASIK, in which a flap is created and tissue beneath it is removed in order to alter corneal topography and hence achieve visual correction(79). Even though the flap is then placed back, it can no longer re-attach fully to the residual stroma, and therefore cannot bear the stresses caused by the external and internal loads applied on the cornea. In comparison to surface ablation techniques, such as PRK, that do not spare the corneal central epithelium, LASIK promotes a fast and almost painless recovery, reduced wound healing response that results in lower rates of haze (corneal opacities) and more predictability and stability in high corrections (80). On the other hand, SMILE is a relatively new procedure that uses a femtosecond laser to create a lenticule inside the stroma without cutting and lifting a flap. The lenticule is then removed through a small, 2-3 mm long, incision leaving the tissue above it mostly connected to the surrounding tissue. SMILE, therefore, has theoretically the same advantages of LASIK over surface ablation procedures, but without the softening of the flap (81, 82). However, it is a relatively new procedure, not as widespread as LASIK and is highly demanding of the laser machine and surgeon experience.

Furthermore, its theoretical advantages still need to be better investigated in mathematical models and studies involving animal experimentation and effects in human subjects.

1.4 Biomechanical Response of LASIK

Corneal tissue removal and flap creation during LASIK are essential steps to achieve corneal reshaping. One inevitable consequence is the resultant corneal softening that can occur after both steps. It has been demonstrated in clinical studies that the flap cutting itself without tissue removal produces corneal softening measured *in vivo*. Gatinel et al. using the Ocular Response Analyzer (ORA; Reichert, Buffalo, NY), observed a reduction in corneal hysteresis and corneal resistance factor after the first hour of flap cutting with a mechanical blade, that kept stable for one month when the flap was lifted and the surgery performed (83). Leccisott et al. using a femtosecond laser to cut the flap observed, before lifting it, corneal softening with an ultra-high speed Scheimpflug camera attached to an air-puff tonometer, the Corvis ST (Oculus Optikgerate GmbH) (84). The corneal softening was also demonstrated in *ex vivo* human corneas, and the amount of softening was related to the side cut angle (85).

If the corneal tissue is softened above a threshold in which it can no longer maintain its shape under the intraocular and external pressures, a bulging (iatrogenic keratectasia) can occur. The first cases of corneal ectasia were described by Seiler in 1998 and he observed that the resulting corneal stromal bed, amount of corneal tissue resultant after laser ablation and flap cutting, had its tangential elastic model reduced to the same level of "natural" occurring ectatic disease such as Keratoconus (86). Later in the same year, he observed that if the cornea presents mild forms of keratectasia at the preoperative a small amount of softening can be sufficient for the progressive form of the iatrogenic induced disease (87). In 2000, in a prospective controlled study, Naroo and Charman observed an association between the amount of tissue ablated from the cornea and the refractive regression due to bulging (88). In the same year, Kamiya et al, also observed an association between the posterior corneal bulging and the residual stromal thickness (89). After that, it was extensively described in the

literature that corneal ectasia can occur even with small changes in corneal tissue during the surgery, and in some cases, previous shape alterations were not identified (17, 90-92).

The resulting corneal shape after the surgery is dependent on corneal biomechanical properties. In severe cases of softening it can lead to iatrogenic ectasia as mentioned, and in less severe softening it can lead to smaller amounts of corneal steepening and regression of the attempted correction. In studies with short and long follow-up periods, it was observed that the higher amount of tissue removed and/or lower corneal thickness at the preoperative which results in lower stromal bed thickness (softer cornea), the regression is more likely to happen (19, 21, 88, 93). In other words, the resulting corneal shape is related to the corneal stiffness, as observed in this thesis.

1.5 Numerical Modelling of Corneal Responses after LASIK

The finite element model (FEM) developed to help solve the design, construction and maintenance of civil structures and mechanical systems, is increasingly being utilised in biomedical sciences, including ophthalmology (23, 94-96).

Most of the numerical models were developed in ophthalmology with applications in refractive surgery. The change caused by the corneal lenticular flap was evaluated in a 3D patient-specific whole eye model by Deenadayalu et al (97). They used an orthotropic material model and observed that the flattening resulting of the flap was higher in softer corneas when compared to stiff ones. However, they did not model the effect of tissue removal. Roy et al created a 2D model of the whole eye in which they considered two different corneal material properties, one soft and one stiff. Their model predicted mild overcorrection in stiff corneas and undercorrection in soft corneas (98). This is in accordance with what was previously observed in clinical studies of myopic regression (steepening) in high amounts of treatment (21). Roy and Dupps, built a 3D corneal-scleral LASIK model using patient-specific corneal topography and predicted the amount of reduction in corneal elasticity after the procedure with inverse analysis comparing the topography obtained numerically and clinically. Even though they considered an enhanced ablation profile, the flap shape was neglected (99). The same

group conducted another study using numerical models comparing LASIK and SMILE, which suggested that SMILE was a relatively safer procedure (100). The same conclusion was reached by Seven et al. comparing contralateral procedures in the same patient flap based tissue removal and SMILE (101). Bao et al. created a patient-specific whole eye 3D LASIK model with enhanced flap architecture and ablation profile. They found that the shape matching of the posterior numerical model and clinical post-operative topography was higher than when they just subtracted the shape of ablation without considering the biomechanical effect. They used Ogden material model to represent the hyperelastic, isotropic and nearly incompressible nature of the cornea with parameters previously described for a single age, 30 years, for all cases (24). No variable corneal material properties were considered in their study (24, 102-104). Until now, a comprehensive analysis of the corneal material properties effects on a complex modelling of refractive surgery with enhanced flap architecture and ablation profile is still missing in the literature.

1.6 Concluding Remarks and Aims of the Thesis

The human visual system is complex and dynamic. Its parts are finely arranged in order to form sharp images on the retinal plane, so it can be transmitted to the central nervous system and properly interpreted. As in most of the biological systems, lots of imperfections are present. This happens even in the normally working eyes. However, these imperfections are disposed of in a way to diminish each other's effects. The most common cause of visual impairment is the low order aberrations or refractive errors, commonly named myopia, hyperopia and astigmatism, which derive from an imbalance between the ocular shape and its dimensions. They can be temporarily corrected by the use of glasses or contact lenses, or they can be more permanently addressed with surgery.

There are several surgical options for correction of refractive errors, among them, LASIK is the most performed procedure worldwide. Corneal response to this laser procedure is highly dependent on its biomechanical properties. Soft or stiff corneas may affect the outcome of the procedure, which was theorised by clinical observations and tested in experimental, clinical and numerical studies.

Numerical modelling of the cornea with finite element analysis is a constantly growing field of research. Numerous different shape and material models were proposed to explain corneal behaviour after refractive surgery. So far, none of them have addressed the corneal material properties as a risk factor in the development of post-surgical ectasia and the varying effect inside and outside a physiological range of corneal stiffness on the response to the procedure. This thesis aims to address these points.

Chapter 2: Numerical Modelling of the Refractive Surgery

2.1 Introduction

This part of the study was focused on reconstructing corneal anterior and posterior surfaces using corneal topography data to build patient-specific finite element (FE) models and simulate LASIK refractive surgeries. Different corneal material stiffness levels were tested in each case. The material that produced the smallest errors between the clinical and the numerical results in terms of anterior curvatures was considered to be representative of the patient's true corneal material properties. Also, the effect of different materials on the final corneal curvature after the procedure was evaluated.

The simulation process was divided into steps. Initially, an idealised model of the human eye using average dimensions was built. Next, patient-specific axial length, corneal elevation and thickness data were used to change the nodes coordinates of the cornea and sclera to match the eye-specific dimensions. One material model was chosen from a range of previously defined human corneal stiffness and the stress free configuration, a virtual state where the intraocular pressure (IOP) is zero, was carried out to obtain a relaxed model configuration (103). The surgery was simulated by removing the tissue as it would be done in the actual procedure. The final step was to re-inflate the eye to its originally measured IOP to obtain the simulated postoperative eye. At this step, correction of the model's corneal thickness is performed to compensate for the lack of information from the surgical procedure. Finally, the comparison between the final numerical anterior surface and the postoperative clinical anterior surface is performed. The process is repeated with different material models and the one with the smallest error was assumed to represent the true material of the eye. In this process, it is also evaluated how the curvature changes with different values of material properties. These steps are described in detail in this chapter.

2.2 Idealised eye model

This study used a custom-built MATLAB programme (105), to construct the idealised eye. As described previously, the corneal shape is dependent on the anterior surface, and the central and peripheral corneal thicknesses (CCT and PCT, respectively). The anterior topography is considered aspheric, with the peripheral curvature flatter than the central. An ellipsoid is fitted to the anterior surface and the CCT and PCT are used as a reference and linearly interpolated to construct corneal thickness. The sclera is considered to have a spherical external shape and its thickness varies according to the region. At the limbus it is considered to be equal to the PCT, it gradually drops to 0.8PCT at the equator, then increases to 1.2PCT at the posterior pole (102).

The 15-noded modified quadratic triangular wedge elements (C3D15H) with nodes located on the corners and on the middle of the edges were distributed in rings along the surface and in layers along the thickness. Boundary conditions were set to simulate the interactions of the eyeball with the orbit and prevent rigid body motion. Movement in equatorial nodes was constrained in the anterior-posterior direction and in the corneal apex and the posterior pole in superior-inferior and nasal-temporal directions.

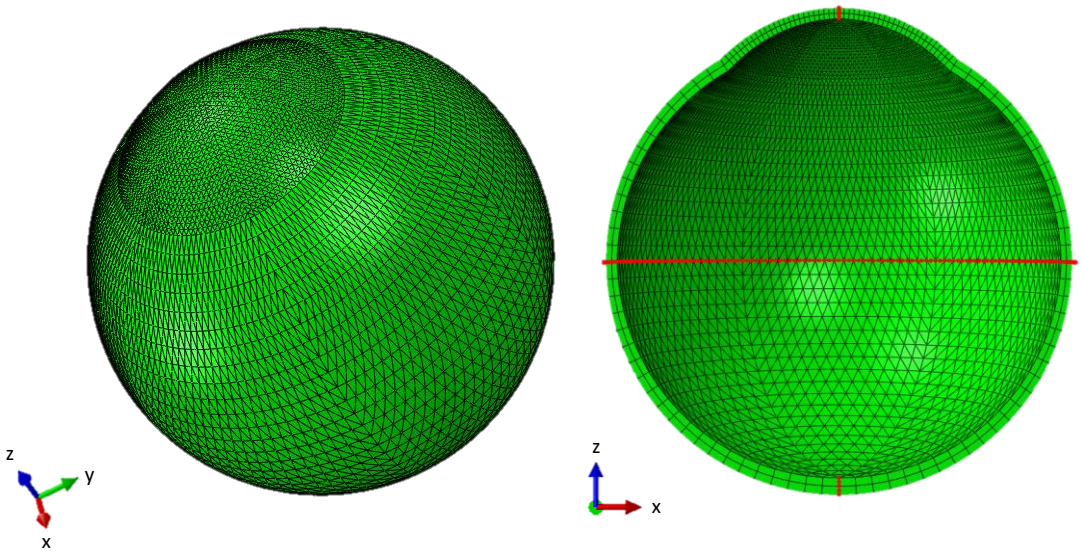

Figure 2 - 1 An idealised eye model, rotationally symmetric, with 60 rings in total (25 rings on the Cornea and 35 rings on the sclera). The corneal and scleral thickness are broken into two layers resulting in 21600 elements. The figure on the right represents a cross-section where the coordinate system is plotted on the bottom left corner. In red the polar and equatorial nodes are marked.

2.3 Surgical parameters

The flap thickness is obtained directly from clinical data. However, the availability of this information is limited and inaccurate because they are manually collected from two cross-sections of the cornea obtained with post-operative OCT images, figure 2-2. In addition, it is possible to observe that the flap thickness in the z-x and z-y cross sections do not intersect each other. Due to these limitations, an approximate estimation of the flap thickness is obtained by fitting the flap data points to second order Zernike polynomials as seen in figure 2 - 3.

Figure 2 - 2 OCT image presenting the flap boundaries.

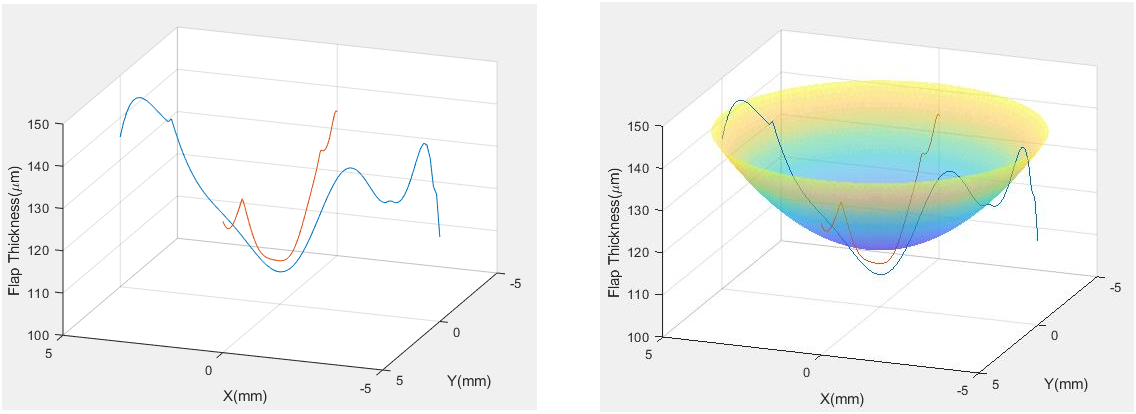

Figure 2 - 3 Cross-section z-x and z-y of flap thickness on the left. On the right 2nd order Zernike expression of the flap thickness.

The complete ablation profile is not available from the laser instrument manufacturer. The ablation profile was defined in a Cartesian coordinate system, calculated based on the depth of ablation at regularly-spaced points along meridians generated at corneal apex, derived using Munnerlyn's formula (106),

$$Ablation\ Depth\ = R_1 - \frac{R_1 \cdot (n-1)}{n-1+ R_1 \cdot D} - \sqrt{R_1^2 - \frac{OZ^2}{4}} + \sqrt{\left[\frac{R_1 \cdot (n-1)}{n-1+ R_1 \cdot D}\right]^2 - \frac{OZ^2}{4}} \qquad \text{(Eq. 3.1)}$$

where R1 is the radius of curvature of the central cornea, n is the refractive index of the cornea (1.376), D is the correction in dioptres and OZ is the diameter of the optical zone of the treatment. The radius of the post-ablated area is obtained by the usual trigonometric approach, using Heron's formula, the variables are illustrated in Figure 2-4.

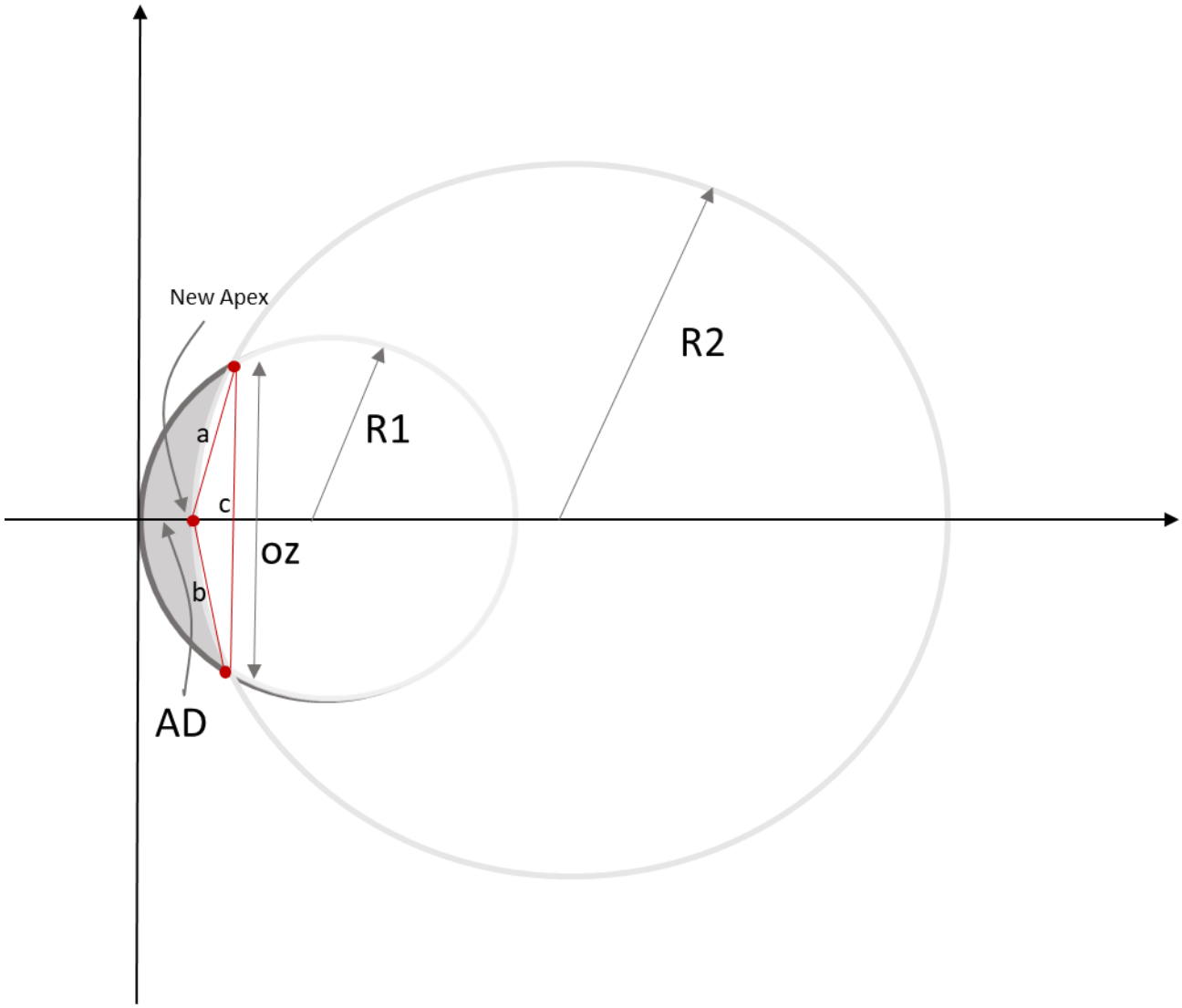

Figure 2 - 4 Post-ablation corneal radius of curvature obtained with the Munnerlyn's formula. AD = Ablation Depth, OZ = Optical Zone, R1 = preoperative radius of curvature of the central cornea, R2 = postoperative radius of curvature of the central cornea, a and b = sides of a triangle connecting the new apex and the two points of interception of the two circles, c = third side of the triangle, equivalent to the OZ.

$$New\ Apex = R_1 - Ablation\ Depth \quad \text{(Eq. 3.2)}$$

$$s = \frac{a+b+c}{2} \quad \text{(Eq. 3.3)}$$

$$R_2 = \frac{abc}{4\sqrt{s(s-a)(s-b)(s-c)}} \quad \text{(Eq. 3.4)}$$

Although it is widely used in clinical practice, the profile obtained with this formula is also a rough estimate, it does not take into account the cornea's asphericity and is frequently underestimated (107, 108). Since the surgical parameters cannot be accurately measured or estimated a correction considering the clinical postoperative thickness is made as will be explained afterwards.

2.4 Patient-specific shape matching

The idealised eye with its boundary conditions is used as the foundation to build the patient-specific shape. A custom-made MATLAB code was developed to read and adjust corneal node coordinates according to the corneal topography and the sclera is stretched according to the axial length. To proceed with this adjustment of node coordinates, the thickness map, anterior and posterior topography are fitted to 10^{th} order Zernike polynomials, so the coordinates of nodes can easily be obtained. Clinical topography data, though, is only reliable in the central area up to 8mm diameter. This makes it necessary to extrapolate data, and the Zernike polynomials are only useful to predict data inside its orthogonal radius. The extrapolation process is then carried out with the fit of the best ellipsoid to the anterior surface, which is not as good as the Zernike polynomials to represent clinical data but it is efficient for extrapolation purposes. The final corneal anterior surface in the model will be formed in the central 8mm diameter area by the Zernike expressions and outside 10mm diameter until the limbus by the best-fit ellipsoid. In the middle zone, from 8 to 10mm in diameter, a smooth transition zone is assumed to connect the two regions, as seen in figure 2-5

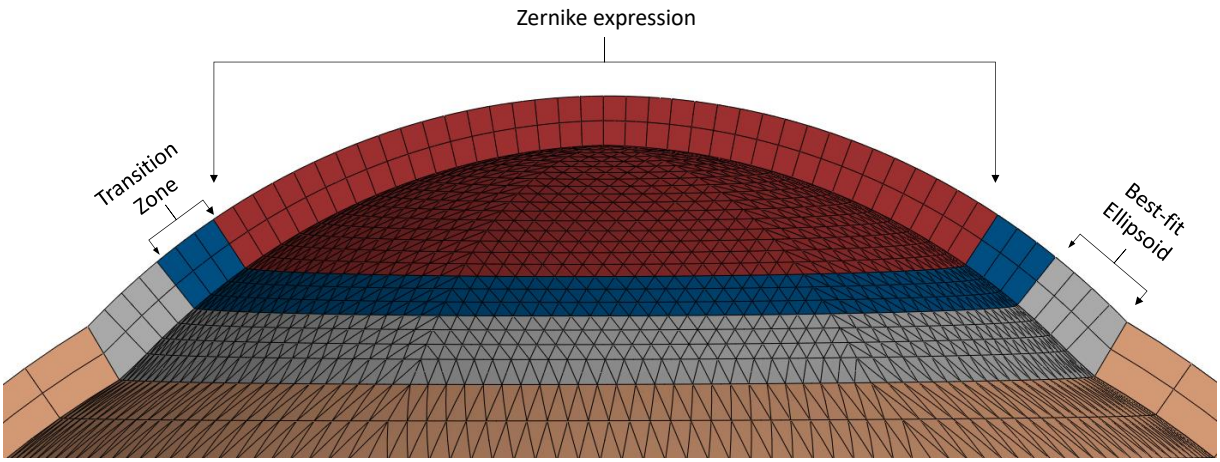

Figure 2 - 5 Schematic view of the steps to implement patient-specific corneal topography and thickness matching in numerical models

This complete method is not adequate to match the thickness map since the best-fit ellipsoid is too simple to represent the complexity of the corneal thickness distribution. The adopted method was to keep the Zernike polynomials to fit the same central area of the thickness map. To predict the rest of the corneal thickness, first, the limbal ring thickness was taken by linear extrapolation of the thickness map and use average values of PCT to simplify the process of representing all the asymmetries of the map at that point. Then the corneal thickness between the Zernike expression area and the limbal ring was linearly extrapolated using data inside the Zernike radius and the predicted PCT at the limbus.

~~To get the posterior surface shape, the anterior surface is taken and the predicted corresponding thickness to each point along the direction of the surface normals is applied.~~ The final step of shape matching, the scleral stretching, is performed by changing the vertical coordinates of the scleral nodes to suit the measured axial length. Figure 2-6 exemplifies this process of changing the idealised eye nodes to the corresponding patient-specific shape.

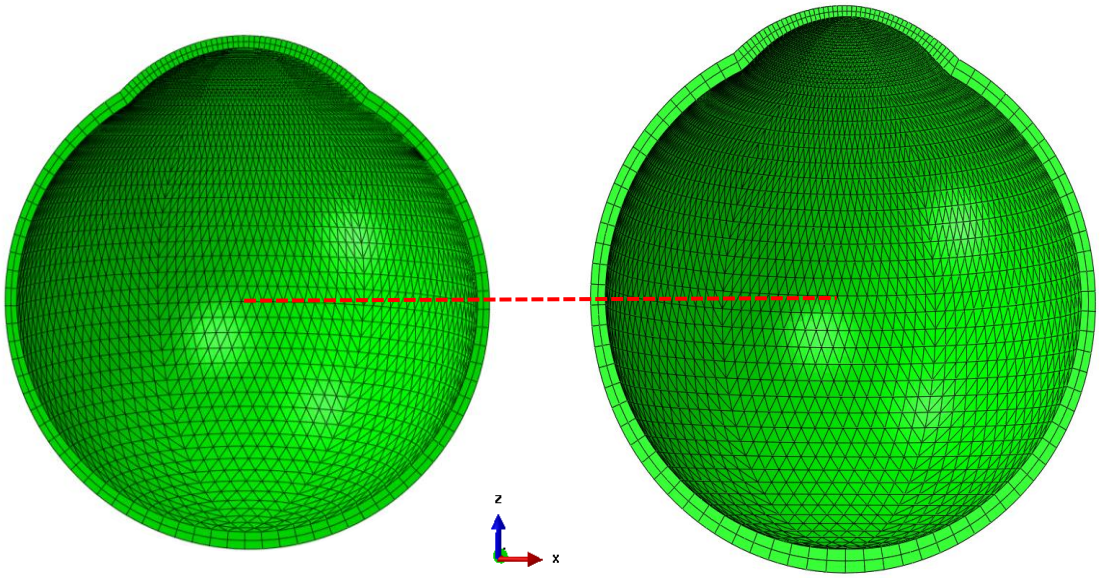

Figure 2 - 6 On the left, the idealised model is represented. On the right, the patient-specific matching of corneal topography and thickness, as well as the scleral stretching.

2.5 Material model

The isotropic Ogden material model was incorporated into the model, so as to simulate the hyperelastic and incompressible nature of the cornea and sclera:

$$U = \sum_{i=1}^{N} \frac{2\mu_i}{\alpha_i^2} \left(\overline{\lambda_1^{\alpha_i}} + \overline{\lambda_2^{\alpha_i}} + \overline{\lambda_3^{\alpha_i}} - 3 \right) + \sum_{i=1}^{N} \frac{1}{D_i} (J_{el} - 1)^{2i} \quad \text{(Eq. 3.5)}$$

where U represents the strain energy potential and $\overline{\lambda_i} = J^{-\frac{1}{3}} \lambda_i$ in which λ_i is the principal stretch and J the total volume strain. The material constants μ_i and α_i define the tissue stiffness and D_i the compressibility of the material, which in this case is set as a very small value close to zero to represent the nearly incompressibility of the cornea and sclera (109).

The μ_i and α_i material parameters values were obtained through inverse analysis modelling described in (105) and the corneal physiological range (10% to 250% of the average of healthy patients) was defined in a parametric study with clinical and experimental validations(110).

The simulation process starts with average material parameters values for cornea and sclera. The scleral material properties are around 5 times stiffer than the cornea. They were held constant during the simulation as this study is interested in corneal deformation and high stiffness of sclera would result in minor variations in deformation with no significant effect on the cornea. Hence by keeping the material properties of sclera the same, optimisation time for corneal material properties significantly decreased while the outcome remained highly accurate. Table 3-2 describes the constants used.

Table 2 - 1 Corneal material parameter constants of cornea and sclera

Tissue	Physiological Range / Regions	Material parameters	
		μ1	α1
Cornea	10%	0.01361	110.83
	25%	0.02614	110.83
	50%	0.03542	110.83
	100% (Average)	0.05399	110.83
	150%	0.06807	110.83
	200%	0.08077	110.83
	250%	0.09224	110.83
Sclera	Anterior	0.27091	150.00
	Equatorial	0.18061	150.00
	Posterior	0.13328	150.00

The epithelium contributes less to the overall stiffness of tissue than the other layers (52). To take this into account a superficial thin layer of 50μm thickness with 10% of the pre-set corneal stiffness (10%μ_1). A model with a specific epithelium layer is shown in Figure 2-7.

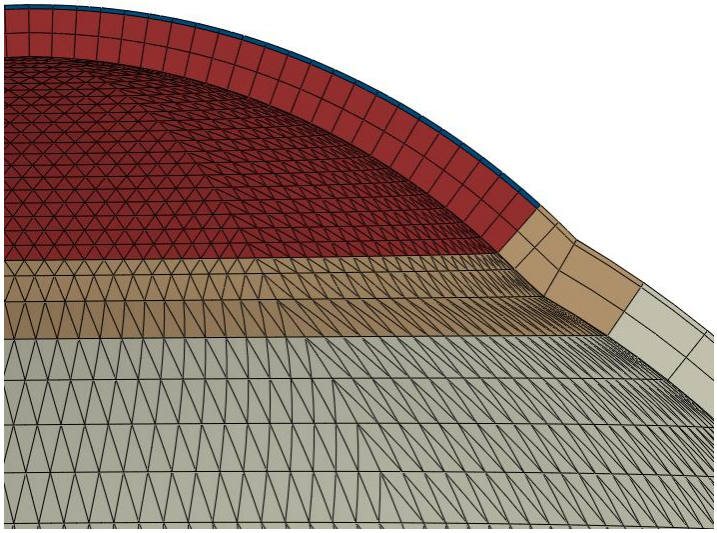

Figure 2 - 7 Model with epithelium layer in blue

2.6 Stress free configuration

The clinical shape measurements are made with the tissue under stresses, which are derived mainly from the IOP (111). It raises two main issues when modelling. One is if it is used directly the clinically obtained stressed shape and re-applied IOP it will overinflate the eye and end up with a bigger model, not representative of the *in vivo* conditions. The other is if the IOP is not applied, the effect of the stresses that exist in the eye will not be accounted, also not being representative of the *in vivo* conditions.

To get the eye's stress free configuration, the virtual shape where IOP is set to zero, the following method described by Elsheikh et al was adopted (112). First, a numerical model, built with the stressed shape X_0 is inflated with IOP. The displacements μ_1 resulting from this process are calculated using non-linear finite element analysis resulting in the shape after inflation x_0. The first estimates of the displacements and of the stress free form X_1 are expressed by

$$\mu_1 = X_0 - x_0 \quad \text{(Eq. 3.6)}$$

$$X_1 = X_0 - \mu_1 \quad \text{(Eq. 3.7)}$$

The following step is to inflate the initial stress free form X_1 and calculate the error vector μ_2 between the inflated shape x_1 and the initial stressed form X_0 for all node positions. The second stress free form X_2 is the result of the subtraction of the error vector μ_2 from the initial stress free form X_1.

$$\mu_2 = X_0 - x_1 \quad \text{(Eq. 3.8)}$$

$$X_2 = X_1 - \mu_2 \quad \text{(Eq. 3.9)}$$

This process is repeated k times and the nodal errors μ_k from the inflated eye x_{k-1} and initial model X_0 are monitored.

$$\mu_k = X_0 - x_{k-1} \quad \text{(Eq. 3.10)}$$

$$X_k = X_{k-1} - \mu_k \quad \text{(Eq. 3.11)}$$

The error estimate of the k_{th} iteration is defined by

$$e_k = \| X_0 - x_k \| \quad \text{(Eq. 3.12)}$$

The iterative process ends when the error estimates e_k are smaller than the tolerance. In this study, 3 iterations have been performed for all cases and the final errors were smaller than the tolerance of 10^{-5}mm. Figure 2-8 describes the iterative process.

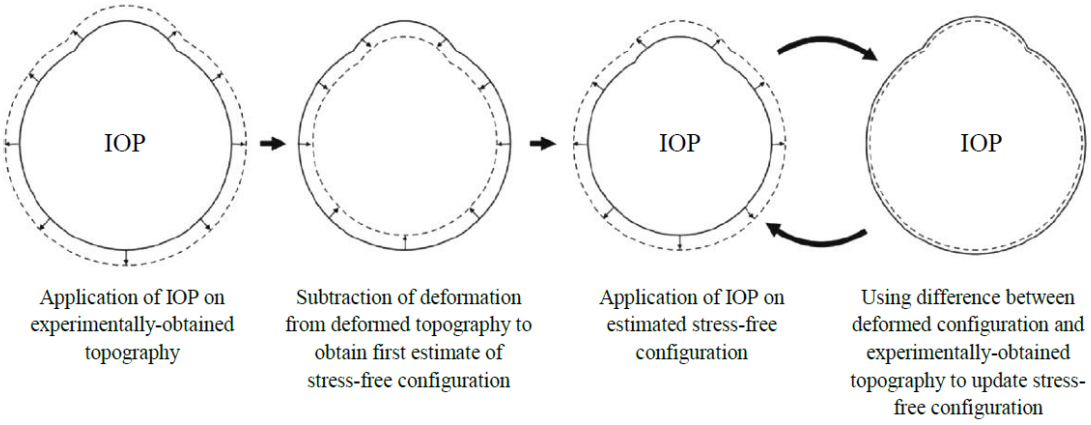

Figure 2 - 8 Schematic description of the iterative process used to obtain the stress free configuration of the eye (112).

2.7 Refractive surgery simulation

In LASIK refractive surgery two main steps are performed: a flap cut and corneal tissue removal with an excimer laser. They were both simulated in the numerical model according to the clinical information as described above. The flap thickness profile fitted to a set of second order Zernike polynomials is used to adjust the thickness of the first two layers (including the epithelium) of the stressed numerical model. The ablation profile mathematically obtained with the Munnerlyn's formula is fitted to fourth order Zernike polynomials in order to allow the assessment of the ablation depth at unsampled locations. This fitted profile is used to introduce a new layer in the stressed model as shown in figure 2-9. At this point, the corneal structure is yet not altered, the tissue that is going to be modified is until now only marked. This is important because when the stresses are removed, the thickness is expected to increase and the diameter to decrease. Since the surgery is going to be performed in the stress free form, the shape alterations are considered in this way.

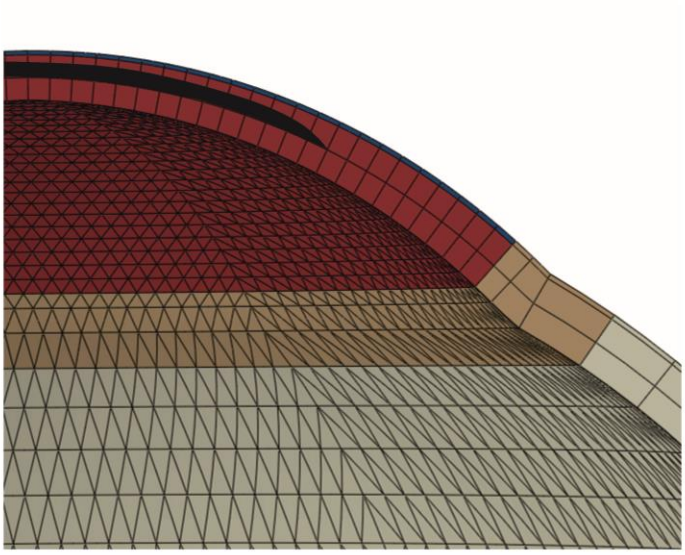

Figure 2 - 9 Ablation layer represents the corneal tissue that will removed with the surgery marked in black

The actual surgical procedure simulation is carried out in the stress free form. The marked layer of the ablation profile is removed from the model and the upper layer's nodes are shifted down accordingly. Next, the first two layers in the central 9mm diameter, corresponding to the flap, is separated from the model. The area that is not cut in the real clinical procedure, called the hinge, is simulated by re-connecting the upper 4mm in arc length region of the flap to the rest of the model using multi-point constraints (MPC). Friction interaction is established in the contact interaction between the posterior flap and the superior residual stromal bed surfaces. The post-operative stress free model is then re-inflated to the full IOP measured clinically.

2.7.1 Thickness correction factor

Because of the approximations adopted in estimating refractive surgery parameters, the resulting numerical thickness did not always match the clinical postoperative thickness. A thickness correction factor was established comparing the postoperative inflated numerical model using the average material parameter (μ_1 = 0.05399) and clinical postoperative shape. This correction factor is then used

to shift the posterior corneal surface inwards in the postopertive stress free model, before re-inflating it. In essence, it compensates for errors associated with flap and ablation measurements.

2.7.2 Error assessment

After obtaining the thickness correction factor with average corneal material properties, the whole process described above is repeated 6 more times for each eye individually. At each repetition, a different value of μ_1 in the predefined range is picked. In all the simulations the same value of the thickness correction is used. The refractive power map of the anterior surface is obtained for all the numerical simulations and for clinical elevation map. The refractive power map was calculated for the front surface (RPf) according to the equation,

$$RPf = \frac{(n_{cornea} - n_{air})}{r_f} \quad \text{(Eq. 3.13)}$$

where n_{cornea} is the refractive index of the cornea (1.376), n_{air} is the refractive index of the air (1), r_f is the radius of curvature of the anterior surface. Even though, regional and interpersonal variations occur in the index of refraction of the cornea, the most commonly used figure of 1.376 is used in the corneal topographer, and to enable comparisons with clinical data, the same value was adopted when calculating the refractive powers of corneal surfaces (113).

The back surface refractive power (RPb) was calculated in a similar way as follows,

$$RPb = \frac{(n_{aqueous} - n_{cornea})}{r_b} \quad \text{(Eq. 3.14)}$$

where $n_{aqueous}$ is the refractive index of the aqueous humour (1.336) and r_b is the radius of curvature of the posterior surface, which will have a negative value. The total refractive power (RP) will be the result of the addition of RPf and RPb.

The clinical assessment of topography is performed with 0.1mm resolution. A value of curvature radius is obtained at every single point of the corneal surface, within 0.1mm distance. The radius of curvature

of the clinical and numerical obtained corneal surfaces are converted to refractive power. The total corneal refractive power is calculated by adding the maps from the anterior and posterior surfaces. The mean total corneal refractive power value is calculated by averaging all points at central 3mm diameter. The mean error is obtained by subtracting the numerical value from the clinical. Averaging the points from the central 3mm diameter.

The material constant that exhibits the lower mean error is considered to represent the true corneal material of the patient.

2.8 Concluding remarks

In this chapter, the numerical simulation of the refractive surgery and how it is used to evaluate the effect of corneal stiffness in the risk of developing post-surgical ectasia and on the final corneal curvature is explained. A patient-specific numerical model of the eye with different corneal material properties was built, the surgery as it would be done clinically was performed and compared to the obtained clinical curvature. By doing that it was possible to obtain the corneal material properties of each eye included in the study and compare the two groups: patients who remained stable after the procedure and patients who developed corneal ectasia.

Chapter 3: Refractive Surgery Effect in Clinical data

3.1 Introduction

In this part of the study the effects of the refractive surgery in the corneal shape are described on the clinical dataset. The review of patients' data submitted to LASIK at the Eye Hospital of Wenzhou Medical University followed the tenets of the Helsinki Declaration of 1964 and revised in 2013. It was approved by the Ethic Committee of the Wenzhou Medical University and written informed consent was provided by all participants (Appendix).

3.2 Patients groups and surgical procedure

Two groups of patients were defined: patients whose corneas remained stable after myopic LASIK surgery and patients who developed iatrogenic ectasia after the surgery, but without signs of the complications identified by the surgeon at the early postoperative – 3 months after the surgery. The inclusion criteria to be part of this study were to not have been submitted to LASIK previously, to present no identifiable signs of pre-surgery corneal shape alterations (subjective surgeon's classification of corneal topography), recorded surgical parameters (maximum ablation depth, ablation and optical zone diameter), low surgical impact (residual stromal bed – RSB>250μm) and to have preoperative and early postoperative (3 months) complete clinical information including complementary examination results of corneal tomography, axial length and OCT measurements of the flap. Corneal tomographic exams were carried out using Pentacam HR (OCULUS Optikgerate GmbH, Wetzlar, Germany), and OCT imaging with Visante (Carl Zeiss Meditec, Dublin, California, USA). Axial length was measured by an A-scan ultrasound device (Compuscan UAB 1000; Storz Inc., St. Louis, MO, USA) and IOP was measured with a dynamic contour tonometer (DCT; SMT Swiss Microtechnology AG, Switzerland).

The LASIK procedure was carried-out as follows, a superior hinged flap was created with a single-use head 90 microkeratome M2 (Moria, Antony, France). The tissue ablation was performed using the excimer laser instrument, WaveLight Allegretto Wave Eye-Q 400 (Alcon, Forth Worth, TX, USA).

3.3 Statistical analysis

Statistical analysis was conducted using the R Core Team (2016), a language and environment for statistical analysis (R Foundation for Statistical Computing, Vienna, Austria; https://www.R-project.org/). The normality of the distribution of the analysed variables was assessed with the Shapiro-Wilk test. Pearson's product moment correlation coefficients along with 95% confidence intervals were calculated to assess the correlation between the corneal changes and the mean spherical equivalent (MSE) treated. A p-value lower than 0.05 was considered statistically significant. Due to the low frequency in which the post-LASIK ectasia occurs and the time between the surgery and the development of the complication being usually long, it is not easy to collect good quality data of these cases and their sample sizes are usually low. The sample size required to determine whether a correlation coefficient differs from zero when $\alpha = 0.05$ and $\beta=0.2$, is 4 subjects when high correlations ($r^2 \geq 0.95$) are expected. Even though, the power of the study (1-β) to find significant correlation when the coefficient presents lower values than mentioned before, reduces with the small sample sizes, a non-significant correlation does not necessarily mean that this correlation is non-existing. According to Goodman: “A nonsignificant difference merely means that a null effect is statistically consistent with the observed results, together with the range of effects included in the confidence interval. It does not make the null effect the most likely. The effect best supported by the data from a given experiment is always the observed effect, regardless of its significance.”(114)

3.4 Clinical characteristics and surgical parameters

In the stable group, 32 eyes of 32 patients were included and 4 eyes of 2 patients composed the ectasia group. Patient’s baseline characteristics and surgical parameters are summarised in Table 3-1.

Table 3 - 1 Clinical Baseline Characteristics and Surgical Parameters of Patients Submitted to Myopic LASIK

	Age (years)	MSE (D)	CCT (µm)	FT (µm)	AD (µm)	OZD (mm)	Ablation Diameter (mm)
Stable	27.1 ± 4.2 (25 -32)	-4.78 ± 1.52 (-8.25 - -1.50)	544.1 ± 27.5 (482 - 604)	123.5 ± 9.5 (103 - 150)	81.8 ± 24.3 (27 - 128)	6.7 ± 0.3 (6.0 - 7.4)	7.8 ± 0.3 (6.9 - 8.4)
Ectasia Patient 1							
OD	45	-5.75	516	98	107	6.5	7.2
OS		-5.25	489	90	98	6.5	7.2
Ectasia Patient 2							
OD	40	-8.75	494	90	135	6.0	7.1
OS		-6.5	500	80	103	6.0	7.1

MSE: Manifest Spherical Equivalent; CCT pre: Central Corneal Thickness of the preoperative; CCT post: Central Corneal Thickness of the postoperative; FT: Flap Thickness; AD: Ablation Depth; OZD: Optical Zone Diameter

At 3 months postoperative the MSE were comparable in both groups. In the stable group it was 0.06 ± 0.29 D (-0.38 – +1.00 D) and it was 0.05 ± 0.39 D (-0.50 – +0.38 D) in the ectasia group.

3.5 Change in anterior corneal power

Figure 3-1 shows the reduction in mean anterior keratometry (ΔK [D]) versus the treatment MSE (tMSE [D]). Results in the two groups were similar and high negative correlations were found. The regression equations for the straight lines in Figure 2-1 are:

$$\Delta K = -0.82 * tMSE + 0.42 \text{ (Stable) } (r^2=0.96\ [0.91 – 0.98]) \quad \text{(Eq. 3.1)}$$

$$\Delta K = -1.08 * tMSE - 0.55 \text{ (Ectasia) } (r^2=0.95\ [0.05 – 0.99]) \quad \text{(Eq. 3.2)}$$

where ΔK (D) is the reduction in anterior keratometric value and tMSE is the treated mean spherical equivalent; r is the product-moment correlation coefficient with the 95% confidence interval. The correlations between ΔK and tMSE were shown to be highly significant ($p<0.001$ for stable and

p=0.025 for ectasia group). The slope of the regression equation close to -1 in both cases represents that the change in anterior corneal power and the intended correction were roughly of the same magnitude in different directions (i.e., the intended correction of MSE of -1 D would produce 1 D of reduction in anterior corneal power, with only mild differences in each group.

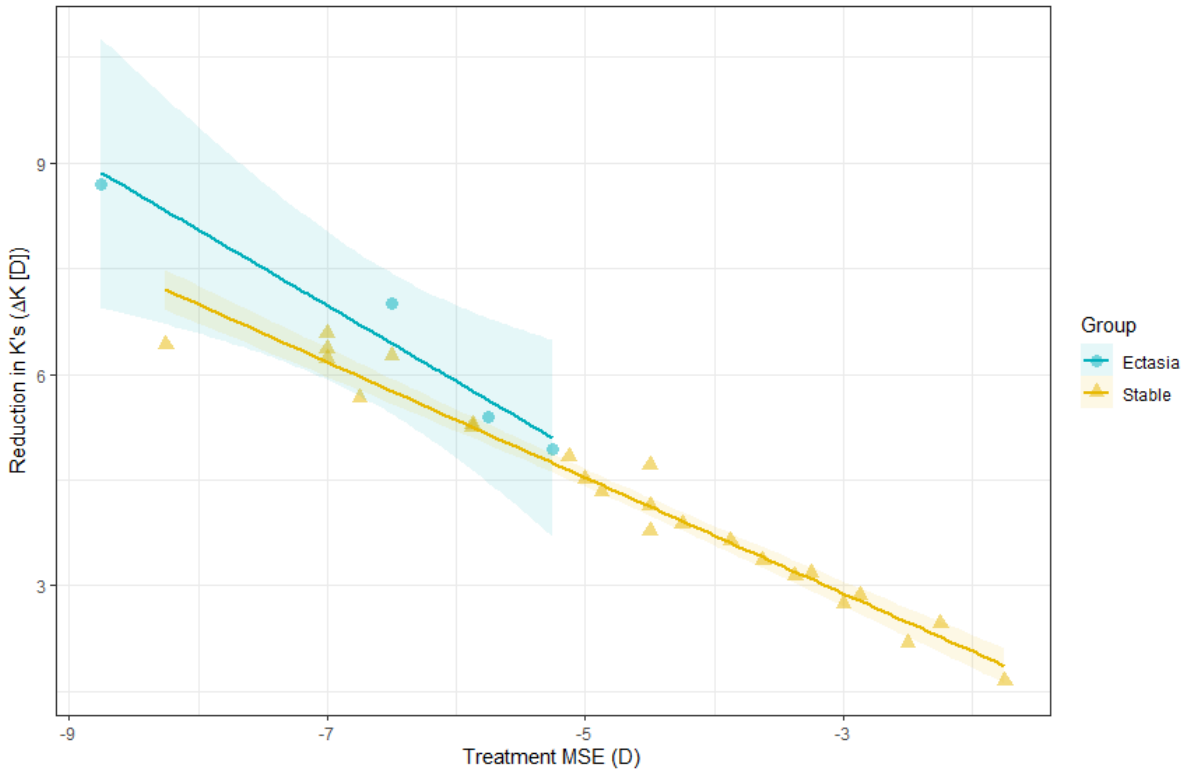

Figure 3 - 1 Early postoperative reduction in anterior corneal power as a function of treatment MSE in patients that remained stable after the surgery and in patients that developed post-LASIK ectasia.

3.6 Change in corneal thickness

The reduction in CCT (Δt [µm]) versus the tMSE is shown in Figure 2-2. It is also observed that the reduction in thickness is negatively correlated with the in intended correction, i.e., the reduction in thickness is higher in cases of more negative corrections. The regression equations for the straight lines in Figure 2-2 are:

$$\Delta t = -12.82 * tMSE + 28.92 \text{ (Stable) } (r^2=0.75\ [0.52 – 0.88]) \quad \text{(Eq. 3.3)}$$

$$\Delta t = -10.28 * tMSE + 43.15 \text{ (Ectasia) } (r^2=0.87\ [0.06 – 0.99]) \quad \text{(Eq. 3.4)}$$

where Δt (µm) is the reduction in central corneal thickness value and tMSE is the treated mean spherical equivalent; r is the product-moment correlation coefficient with the 95% confidence interval. The correlation between Δt and tMSE was found significant in the stable group ($p<0.001$) and barely significant in the ectasia group ($p=0.064$). Even though, the significance level to reject the null hypothesis wasn't reached and the confidence interval was large in the small sample that compose the ectasia cases, the slopes of the regression lines and the correlation coefficients were very similar and pointing to the same trend of the stable cases.

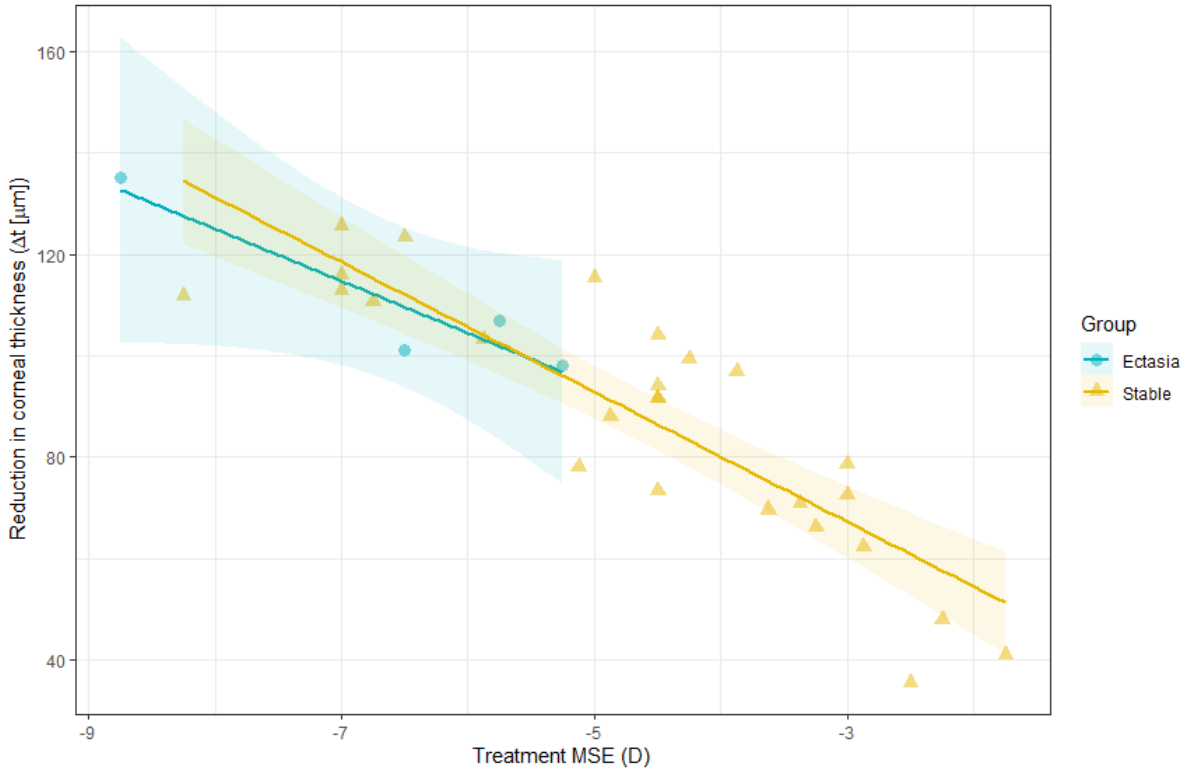

Figure 3 - 2 Early postoperative reduction in corneal thickness as a function of treatment MSE in patients that remained stable after the surgery and in patients that developed post-LASIK ectasia.

3.7 Change in posterior corneal radius of curvature

The posterior corneal surface has a negative refractive power due to the smaller index of refraction of the aqueous humour when compared to the corneal index of refraction. In order to better evaluate the shape modifications, the change in the central 3mm posterior radius of curvature in mm versus the tMSE is presented in figure 2-3. The regression equations for the straight lines in figure 2-3 are:

$$\Delta r = 0.02 * tMSE - 0.04 \text{ (Stable) } (r^2=0.45\ [0.17 – 0.68]) \quad \text{(Eq. 3.5)}$$

$$\Delta r = 0.07 * tMSE + 0.19 \text{ (Ectasia) } (r^2=0.83\ [0.15 – 0.99]) \quad \text{(Eq. 3.6)}$$

where Δr (mm) is the change in posterior radius of curvature and tMSE is the treated mean spherical equivalent; r is the product-moment correlation coefficient with the 95% confidence interval. The correlations between Δr and tMSE were significant for the stable group ($p<0.001$) and barely significant for the ectasia group ($p=0.088$). In opposition to the flattening observed in the anterior corneal surface by the reduction of the refractive power, it is observed steeping in the posterior surface by the decrease in posterior radius of curvature. Even though, the significance level to reject the null hypothesis wasn't again reached and the confidence interval was large in the ectasia cases, the higher slopes of the regression lines in this group point towards the direction of higher posterior steepening observed in these cases.

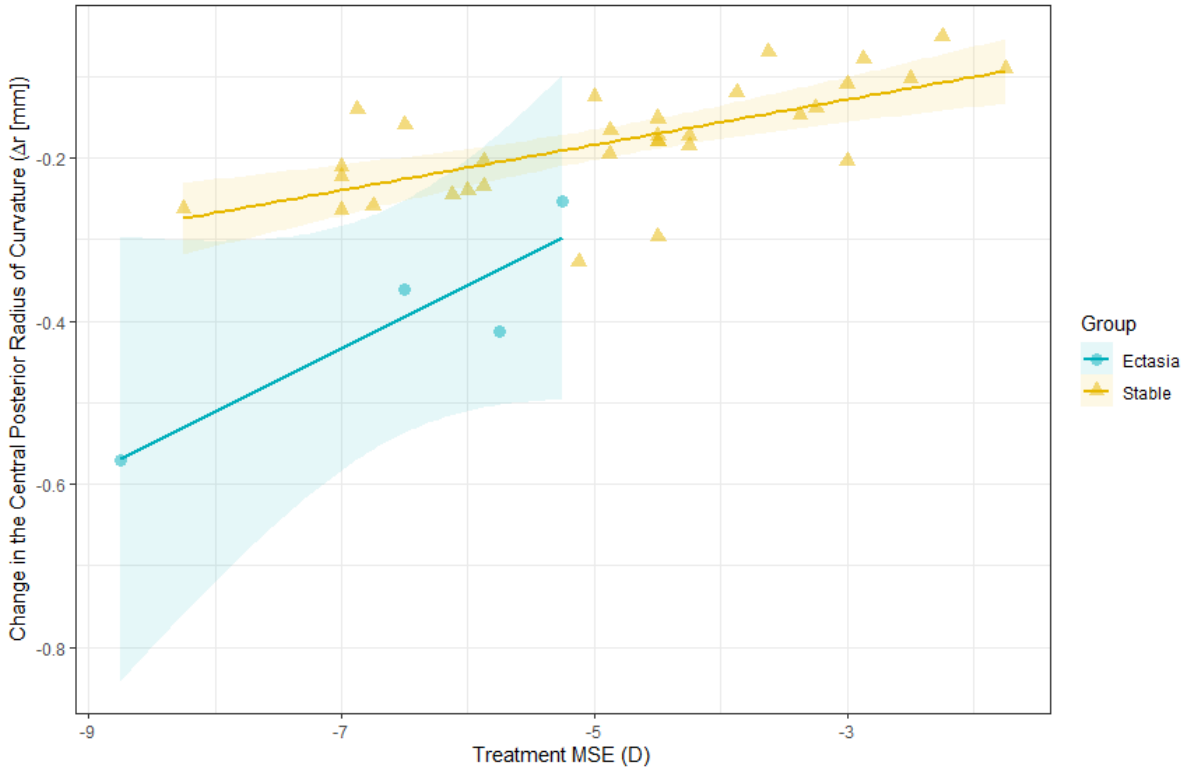

Figure 3 - 3 Early postoperative change in central posterior radius of curvature as a function of treatment MSE in patients that remained stable after the surgery and in patients that developed post-LASIK ectasia.

3.8 Concluding remarks

In this chapter, the effects of the refractive surgery on the corneal shape were evaluated. Similar trends were observed in both groups regarding the amount of flattening and thinning in relation to the amount of treatment. Corneal steepening was observed in the posterior surface in both groups, and it was more intense among the patients that developed post-LASIK ectasia. It is important to acknowledge that the small size of the ectasia group is a limiting factor of this analysis and the trends observed may not necessarily be confirmed in bigger samples.

Chapter 4: Determination of Patient-Specific corneal material properties by means of numerical and clinical data

4.1 Introduction

The changes in raw elevation maps are subtle, therefore its use by clinicians is not practical (115). The power maps are easier to interpret and are widespread in clinical practice (116). In addition to that, the goal of the laser vision correction surgery is to change the refractive power of the cornea so that the light rays can be focused on the retinal plane. The results in this section present the corneal refractive power in the central 3mm diameter zone with different corneal stiffness levels. The central corneal curvature values were chosen because they are more reliable and the usual exam coverage does not include the periphery (117). First, the curvature error between each simulation and the clinical value was evaluated for each eye in the study in order to evaluate the patient-specific corneal material properties and then compare it between the groups.

4.2 Statistical analysis

The main outcome of the thesis was the evaluation of the corneal material properties differences between the stable cases and the cases that developed ectasia. Sample size was calculated from a previous pilot study conducted by the BioEG group from the University of Liverpool (Elsheikh et al., unpublished data) in which the corneal material properties of healthy patients were compared with patients with corneal ectasia. To confirm a expected difference of 0.6 in standardised corneal material properties with a standard deviation of 0.4, power of 80%, and significance level of 5%, keeping a proportion of patients that developed ectasia for patients that remained stable of 1:8 (since the surgical complatication is a rare event), the sample size should consist of a minimum of 36 eyes (4 eyes that developed ectasia and 32 eyes that remained stable). The statistical analysis was conducted using the R Core Team (2016), a language and environment for statistical analysis (R Foundation for Statistical Computing, Vienna, Austria; https://www.R-project.org/). The normality of the distribution

of the analysed variables was assessed with the Shapiro-Wilk test. Student's t test was used to evaluate the differences between the groups. A p-value lower than 0.05 was considered statistically significant.

4.3 Simulation results

The simulation will be exemplified in one patient with average ocular dimensions that remained stable after the surgery. The right eye of the chosen patient who was a 25 years-old female treated for -4.50D (MSE) is shown. The process starts with adjusting the idealised eye to the patient-specific shape and axial length. Figure 4-1 illustrates this matching process in a single patient.

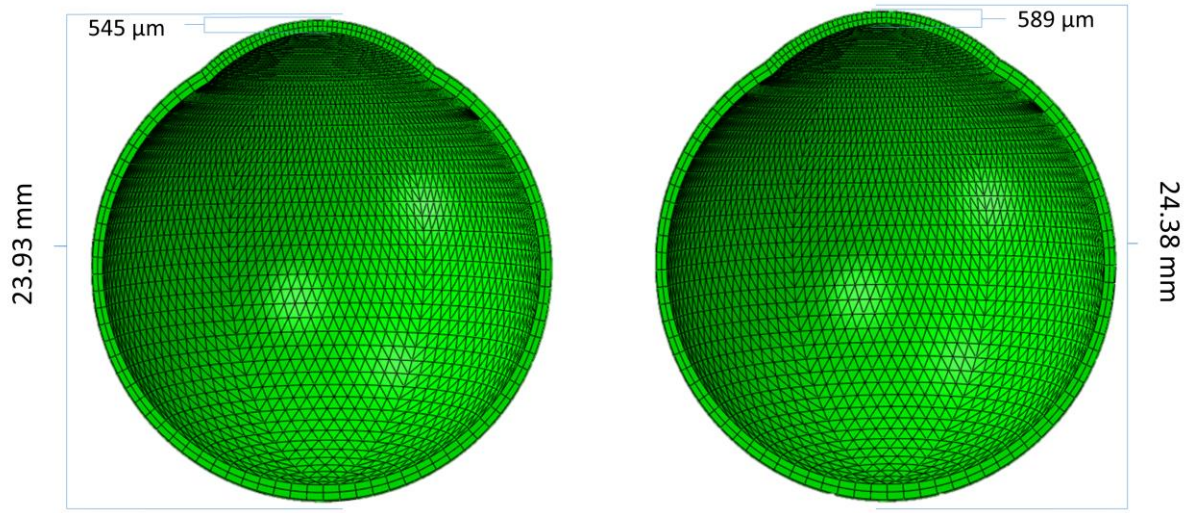

Figure 4 - 1 On the left, idealised eye dimensions. On the right, corneal curvature and axial length matched to patient-specific information

Central refractive power change from the idealised eye to the clinically match numerical mesh is observed in figure 4-2 for the same patient.

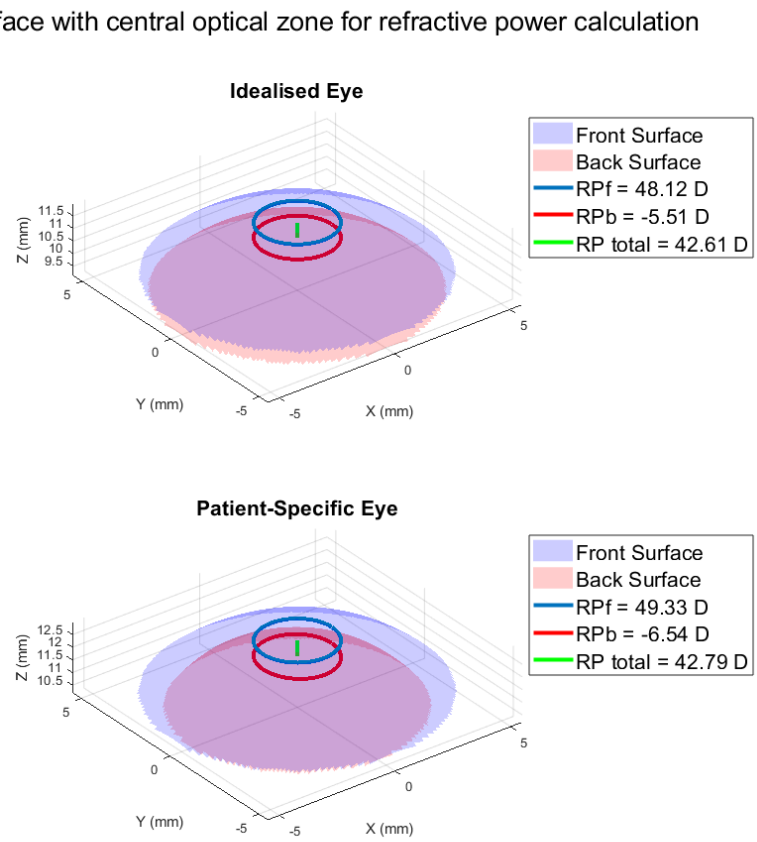

Figure 4 - 1Corneal Surface with central optical zone for refractive power calculation marked with circles. RPf = refractive power of front surface; RPb = refractive power of back surface, RP total = RPf + RPb.

The next step of the simulation is to obtain the stress free configuration considering the average material, where the eye becomes smaller and thicker as observed in figure 4-3.

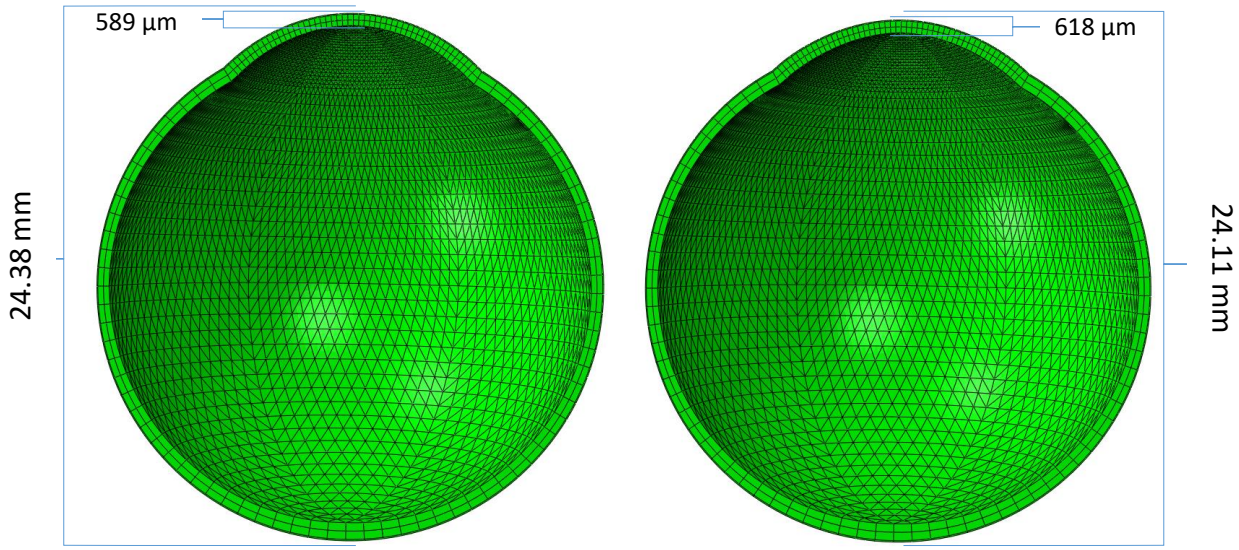

Figure 4 - 2 Stress free form of a single patient's eye. On the left the original patient's axial length and corneal thickness. On the right the shortening and thickening resulting from the process of removing the stresses.

The corneal tissue is removed and the flap is detached at this stress free stage according to estimated parameters based on the clinical information.

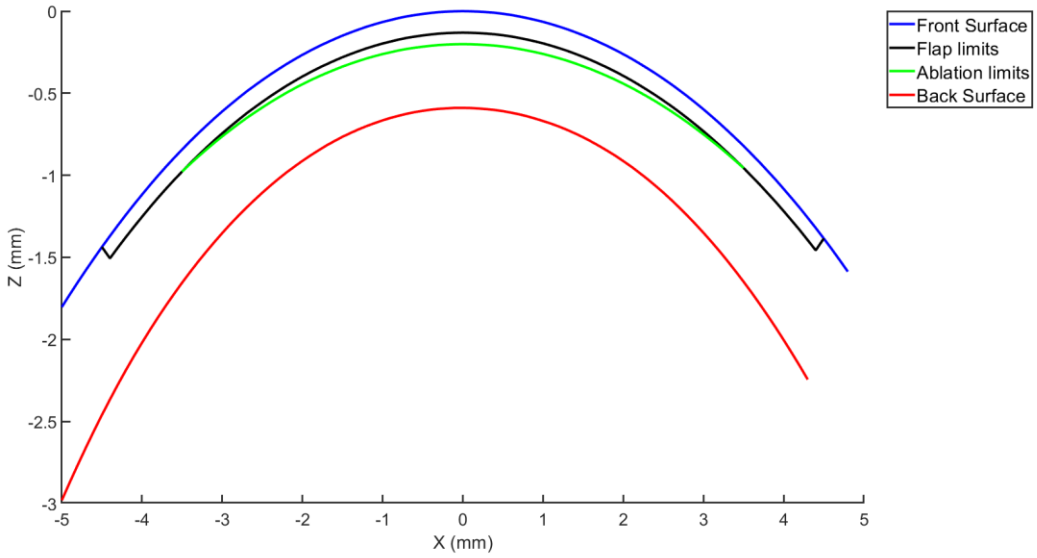

Figure 4 - 3 Corneal cross-section evidentiating the surgery parameters (Flap and Ablation) estimated based on clinical information of the patient used in the example.

The final model after surgery has been introduced and is inflated to the measured IOP using static analysis in Abaqus. It is observed in figure 4-5 that the flap, apart from the hinge area, which is the only part that is still attached to the rest of the corneal tissue, carries almost no stress. The displacement as expected is higher oposite to the hinge area as observed in figure 4-6.

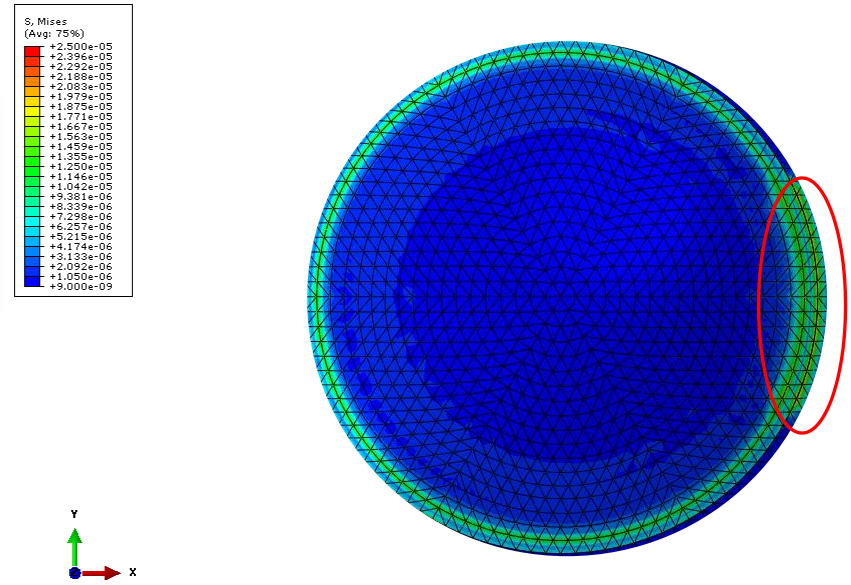

Figure 4 - 4 Stress distribution over the flap area at the central cornea.

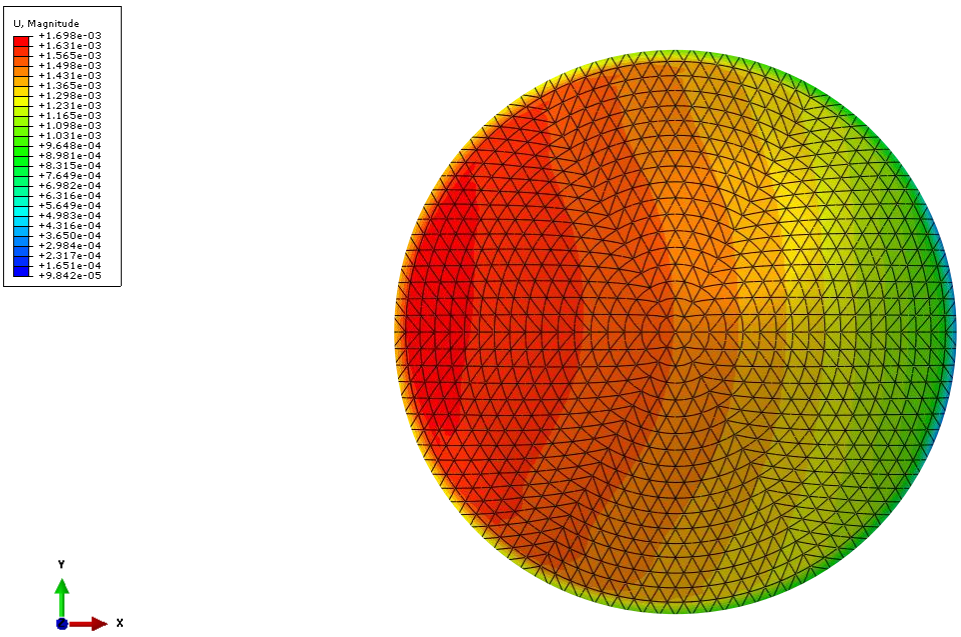

Figure 4 - 5 Displacement distribution over the flap area at the central cornea.

After generating this patient-specific final model and simulating the surgery, its post-surgery thickness was compared with the clinically measured central corneal thickness. Since the surgical parameters are not fully available, certain approximations were adopted. A thickness correction factor is defined to shift the models' posterior surface. However, the curvature is not altered, as observed in figure 4-7.

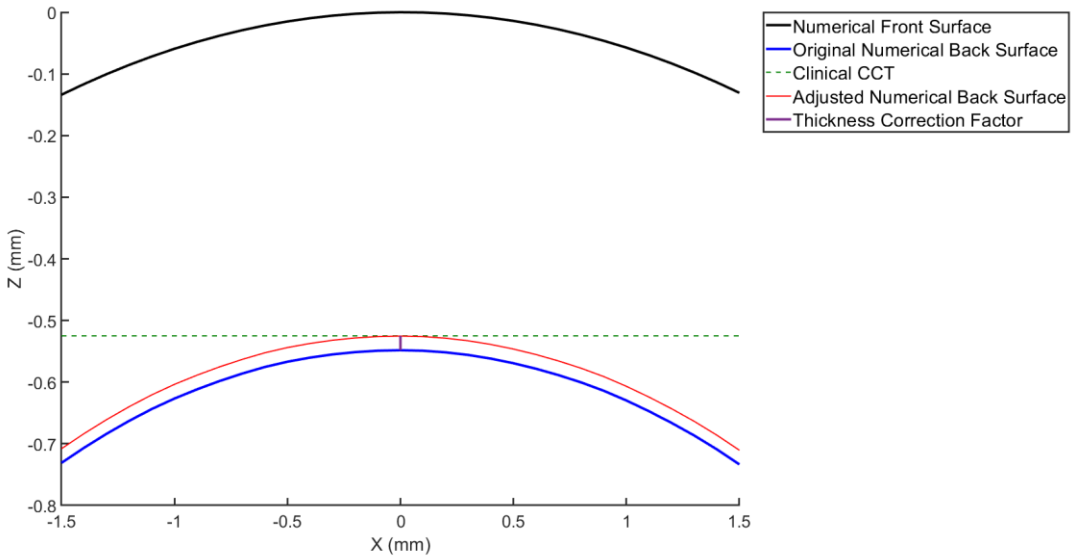

Figure 4 - 6 Comparison of numerical and clinical postoperative central corneal thickness (CCT) and estabilishment of thickness correction factor.

The final step of the process is, after applying the correction factor, to compare the curvatures of the numerical and clinical models and calculate the mean error. Figure 4-8 exemplifies the final output of the process and the error calculation.

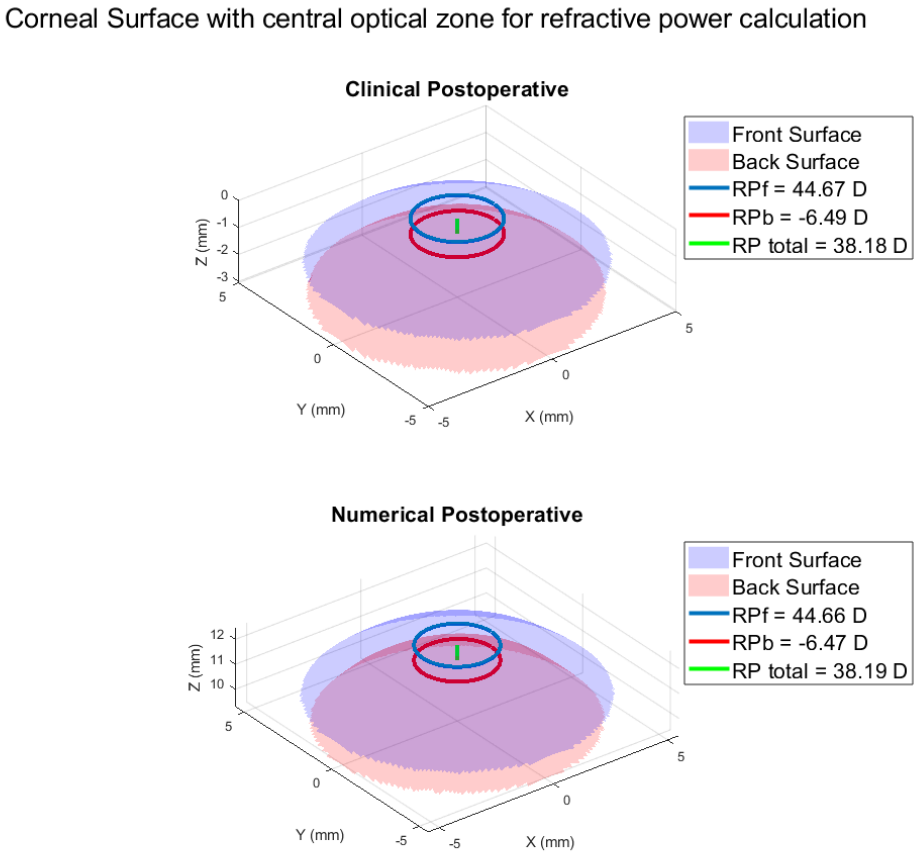

Figure 4 - 7 Comparison of final central refractive power and calculate the mean error. In this specific case it was -0.01D.

4.3 Corneal material properties as a risk factor for post-LASIK ectasia

The process described in the last section is repeated 6 more times with different corneal stiffness levels. The thickness correction factor, however, is kept the same as the one obtained with the average corneal stiffness (μ = 0.05399). The material parameters were expressed as a percentage of the average corneal stiffness, with 1 representing the previously described average physiological corneal stiffness by Eliasy et al. (Unpublished data). The same group also described the physiological range between 0.5 and 2.5, regarding the average corneal material parameters. The mean central refractive power obtained with each material parameter is subtracted from the mean clinical refractive power

and a curve is interpolated using cubic spline method. The point where the error is closest to zero is representative of the corneal stiffness of the patient. Figure 4-9 illustrates this process in the single patient, whose data was used in the example.

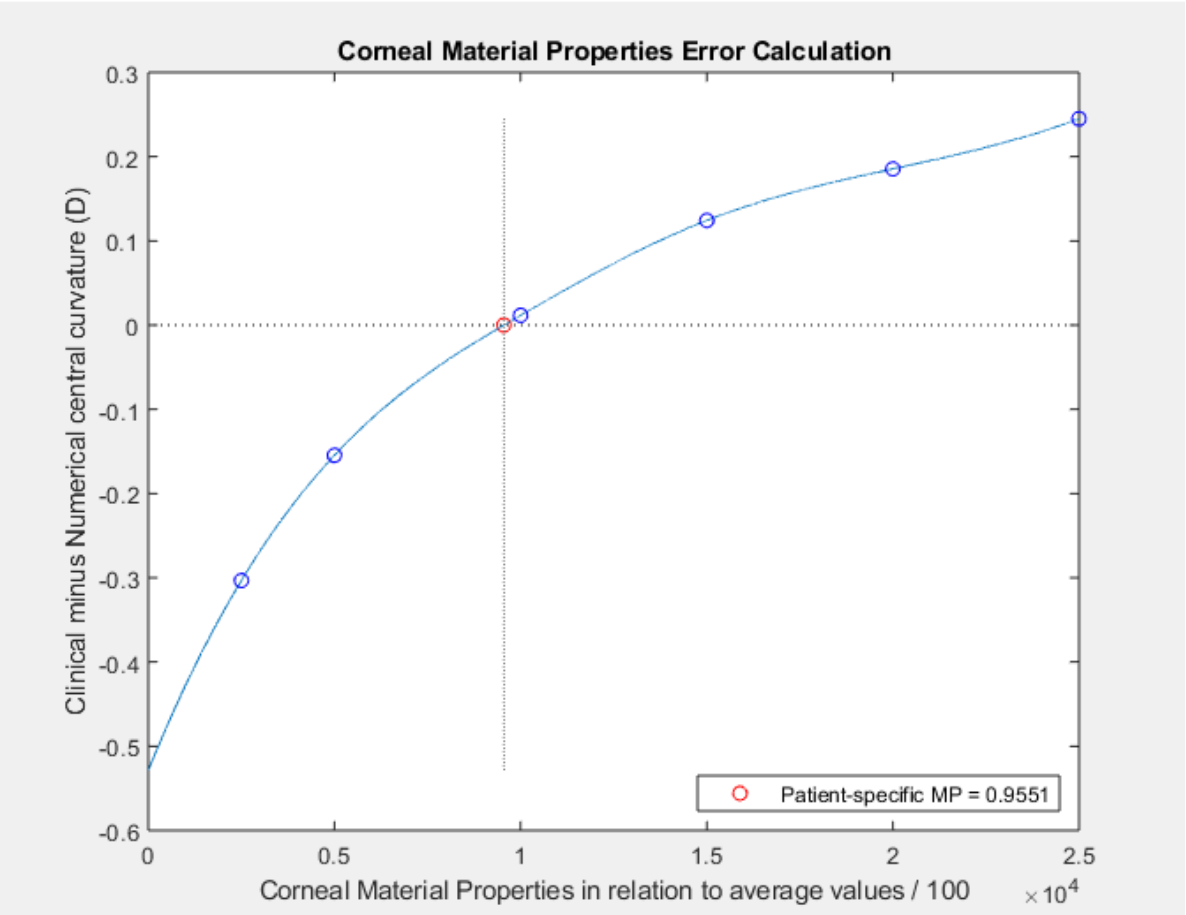

Figure 4 - 8 Error calculation of the refractive power map to define the patient-specific corneal material properties.

The stable group, as previously described, composed of 32 eyes from 32 patients, presented corneal material properties of 1.2 ± 0.6 and the average value of the ectasia group (4 eyes of 2 patients) was 0.3 ± 0.2. Figure 4-10 demonstrates the group's distribution.

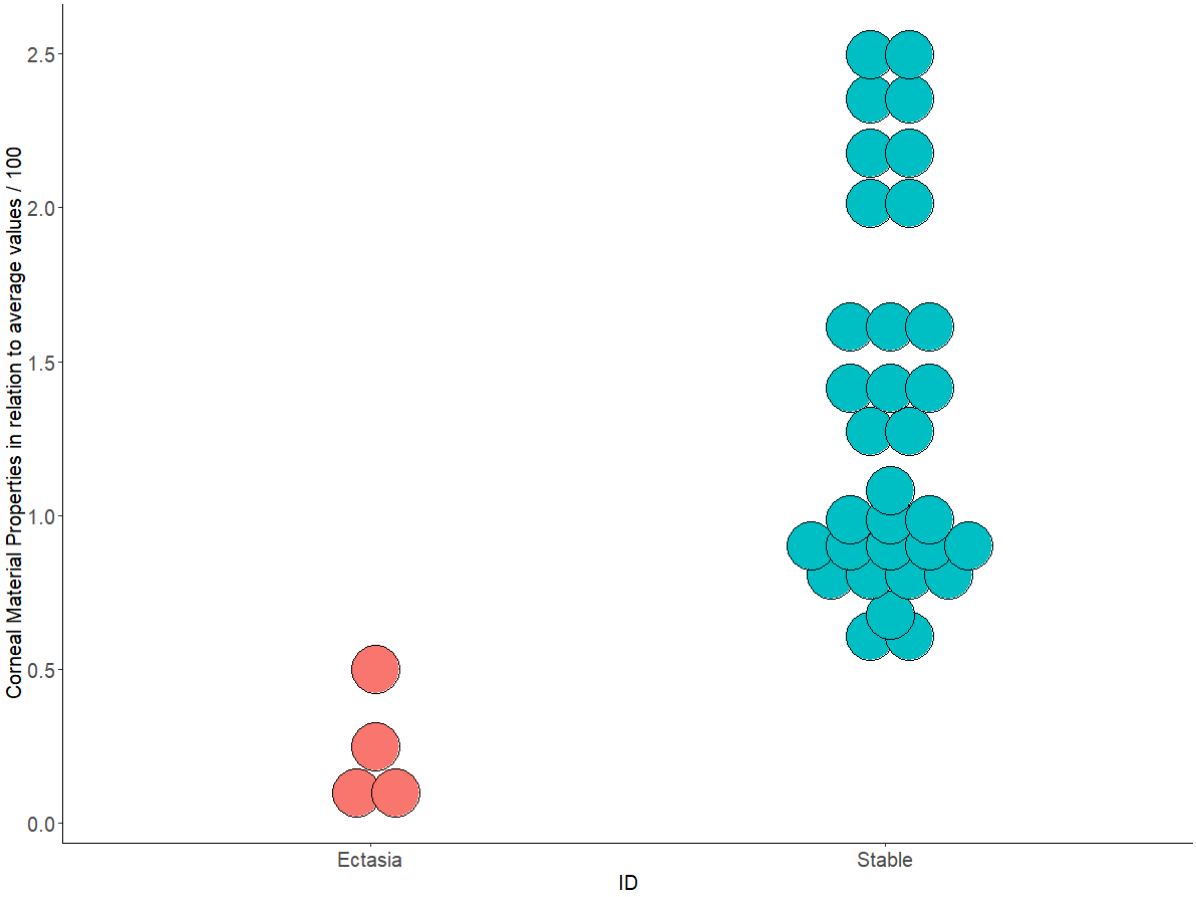

Figure 4 - 9 Corneal material properties distribution across the groups.

4.4 Effect of corneal stiffness on corneal curvature

Considering all cases, the change in corneal curvature in relation to the corneal material stiffness is seen in figure 4-11. In the range of normal values from 0.5 to 2.5, the 0.6D variance was observed.

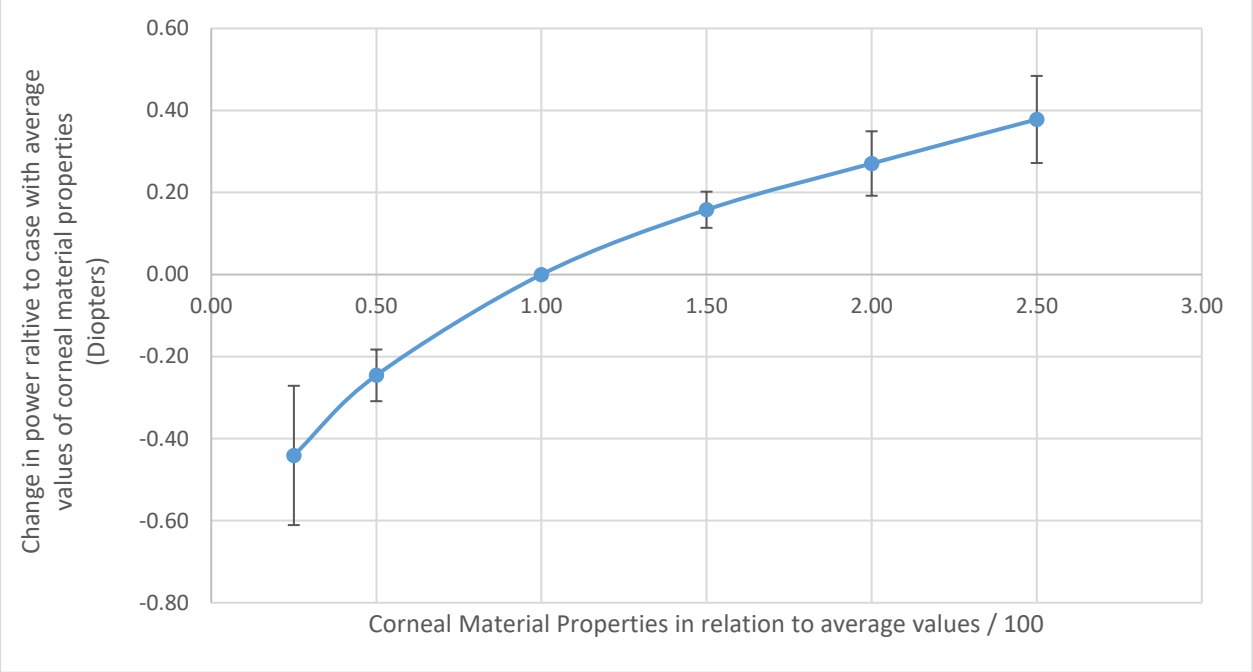

Figure 4 - 10 Change in power according to the corneal material properties.

Chapter 5: Discussion and Conclusion

5.1 Introduction

In this chapter, the results are discussed regarding the corneal shape alterations with refractive surgery, differences in corneal stiffness between the groups and its effects in corneal curvature are discussed. Limitations and future plans are delineated, and conclusions of the study are drawn.

5.2 Corneal shape changes after refractive surgery

Similar trends were observed in flattening of the anterior surface and corneal thinning between stable and post-LASIK ectasia cases. On the posterior surface, even though statistical significance was not reached, there was a difference in trend. The stable cases presented only mild posterior steepening, while in the ectasia cases this steepening was more pronounced.

The first reports of posterior alterations changes after refractive surgery using a slit-scanning tomographer, the Orbscan, observed a frequent forward shift of this surface(88, 89, 118-120). Later

studies using different technologies suggested a present but milder forward shift of the posterior surface (121-123). Most of the studies reported the steepening in terms of relative elevation rather than posterior radius of curvature. Naroo et al, reported reduction in posterior best-fit sphere (BFS) radius measure with the Orbscan ranging from 0.6 to 1.8 mm. Hashemi et al, also reported reduction in posterior BFS radius, but found lower values. In their study, using newer versions of the tomographers, the maximum reduction on the BFS measured with Orbscan II was 0.31 mm and with the Pentacam 0.25 mm. In this study, the reduction in the posterior surface radius of curvature is consistent with the more recent results. The observation of a different trends between the two groups suggests that this higher steeping can be an early sign of the complication, however, the results should be interpreted with caution due to the absence of statistical significance and this result needs to be replicated in a bigger sample. Another point to be considered is that post-LASIK ectasia is a late complication. The average time reported by Randleman et al. was 15.3 months with only one-third of the cases presenting the ectasia before 6 months (124). Bohac et. Al reported an incidence of 10 cases of ectasia in over 30,000 cases operated. In their series the earliest onset was 8 months and the average time of occurrence of the complication was 3.8 years (125). In this study only early postoperative was evaluated and big alterations in the posterior surfaces weren't expected.

5.3 Corneal Biomechanics as a risk factor for post-LASIK ectasia

To the best of our knowledge, this was the first study to evaluate the corneal material properties as a risk factor for iatrogenic ectasia. The concept has been addressed since the first reports, but so far, no study was able to demonstrate it, as was done in this thesis. The main reasons are that it is extremely difficult to get the patients to include in the study, there was no proper method for evaluating the corneal material properties *in vivo* and systematic corneal material parameters with close relation to the human tissue to be used in the numerical models hadn't been established yet.

5.3.1 Post-LASIK ectasia mechanisms

The corneal post-LASIK ectasia is a multifactorial complication, however, it is known that there is a biomechanical failure of the tissue (126). It can happen if the tissue was already soft or if it was considerably softened by the surgery with resulting low residual stromal bed or by repeated trauma during the postoperative period, such as eye rubbing (86, 87, 108, 127). While devastating, it is usually infrequent, with an incidence ranging from 0.04 to 0.9% (90, 128-130). Sometimes it may take 11 years for its onset (131). All of that makes it hard to get good quality patients' records and exams to study.

In this study, it was possible to get complete information on 4 eyes from 2 patients that developed the complication without commonly reported risk factors such as alterated topography or low RSB. This includes clinical records, information about the surgical parameters such as the programmed flap thickness and attempted myopia correction, along with tomographic exams, including information on both corneal surfaces and the thickness profile, from the pre and the early postoperative. This kind of technology to measure the posterior corneal surface wasn't available until the mid-2000s, so previous publications only took into account the front surface and the central corneal thickness data, therefore not suitable to build accurate numerical models. There are very few publications evaluating case series of patients that developed post-LASIK ectasia with whole cornea information from the pre and the postoperative. Bühren et al. reported tomographic findings of 10 eyes from 5 patients that developed post-LASIK ectasia (132). However, the authors did not report initial postoperative corneal characteristics. In a previous work, the author could evaluate data of 71 eyes from 45 patients, but since the purpose of the study was to improve the current preoperative method, attention was given to the preoperative exams and early postoperative was not evaluated (17). As the event is not frequent, collecting this early good quality postoperative data was the main limiting factor to increase the sample size.

In clinical practice, corneal softness is usually identified based on changes present on the power maps (91). They are a good indication but are not highly correlated with the tissue stiffness. This can be

observed by the numerous cases that developed ectasia without evident corneal curvature alterations (17, 132). Or by cases with clear alterations that remained stable over the years spontaneously or even after refractive surgery (133). Currently, there are two devices commercially available to measure corneal biomechanics *in vivo*, the Ocular Response Analyzer (ORA; Reichert, Buffalo, NY) and the Corvis ST (Oculus, Wetzlar, Germany). They are both non-contact air-puff based tonometers that evaluate the corneal deformation. The first takes indirect measures of corneal deformation through the incidence and reflexion of the infrared light (134). The second has an ultra-high speed Scheimpflug camera that can capture the actual corneal movement at the horizontal cross-section (135). They both, in their available software, present measures that are also not related to standard mechanical properties.

The ORA has two types of indices: indices derived from the pressures, at which applanation occurs and indices related to the waveform. Among the pressure-derived indices is *corneal hysteresis* (CH), obtained from the difference between the first and second applanation pressures (P1 and P2, respectively) and the corneal resistance factor (CRF) which equals P1 – k*P2, where k is a constant. This constant was empirically developed to increase the correlation of CRF with CCT (134). Both indices are reduced in keratoconus and after refractive surgery (136). Conversely, there was a large overlap in the distribution of CH and CRF between healthy corneas and corneas with mild forms of ectasia , even though the overlap was lower than that observed with standard metrics such as corneal curvature and thickness (137). Luz et al. tested the pressure-derived parameters in forme fruste keratoconus cases and found no statistically significant differences between this group and healthy corneas (138). However, the authors identified significant differences between the two groups in some waveform derived parameters, but with large overlaps and low discriminating ability. The area under the first peak, which was the index that presented the best accuracy to discriminate between the two groups, had area under the ROC curve of 0.717 (138). As single parameters, the ORA indices have limited reliability in the diagnosis of corneal ectasia and in the screening of refractive surgery candidates (139). However, a combination of parameters from ORA and tomography was more

promising in detecting susceptible cases and provided AUC of 0.953, which outperformed individual parameters (138).

The Corvis ST represented an evolution in terms of biomechanical evaluation, since direct visualisation of the cornea under deformation was possible (140). Even though the discriminant ability of individual deformation parameters was also not sufficient to separate the ectasia from the healthy cases, combinations of parameters (leading for example to the Corneal Biomechanical Index, CBI and Tomographic Biomechanical Index, TBI) showed better reliability (141) especially in the detection of very early cases (142, 143).

Despite both ORA and Corvis ST being able to measure corneal biomechanics *in vivo*, there was still a lack in their ability to measure standard mechanical properties such as the tangent modulus. Their measures are also influenced by confounding factors that include the intraocular pressure and corneal thickness (144).

Recently, the BioEG group from the University of Liverpool developed a method to obtain the full stress-strain curve using the Corvis ST data through inverse analysis (110). The method that we used in this thesis can be related to the method proposed by the group. Future perspectives will involve the correlation of the two methods to allow the use the corneal material properties as a proper screening parameter before laser vision correction surgery.

The use of corneal material properties during the preoperative will fill a gap in the current screening strategy. So far, alterations that resemble the corneal ectatic pattern on the anterior surface power map, on the posterior surface relative elevation and on the thickness profile are used as risk factors to counter-indicate the refractive surgery (145). Some attempts have been made to characterize the biomechanical fragility of very early disease cases with in vivo measurements (142, 146). These cases would serve as a surrogate population of the post-LASIK ectasia, but there is still lots of controversies if those cases are really at high risk of developing the complication or not (147).

5.3.2 Corneal material models

There are several numerical simulations of the refractive surgery described in the literature developed with the purpose of evaluating corneal softening after the procedure or the previous soft status as a risk factor (85-92). However, the material constants on these studies are derived from inverse analysis using previous healthy cornea data and they usually report consequences of the material behaviour such as displacement. They did not consider the tissue material properties as an individual risk factor for the complication.

The study on corneal material properties conducted by BioEG group has established optimized constants for the corneal material model that are consistent to actual clinical scenarios (110). This made it possible to test the material parameters as a risk factor for the development of ectasia and the effect that corneal stiffness has on the final surgical outcome.

We observed that the normal eyes presented corneal stiffness inside the normal range as described by Eliasy et al. from 0.5 to 2.5 (110). From the ectasia cases, 3 eyes presented corneal stiffness lower than the normal range and one eye was borderline regarding the lower limit of this range (0.5). These results are in accordance with the above-discussed theory that the previously present corneal softness would be an important predisposing factor to post-LASIK ectasia.

The study presented in this thesis has a few limitations. The number of cases with ectasia is low (4 eyes), and even though a good study power was reached for the main outcome (differences in corneal material stiffness between stable and ectasia cases), the power to evaluate curvature changes was not enough to draw stronger conclusions. In terms of modelling of the refractive surgery, the laser manufacturers did not provide full information about the ablation profile. Further, for the flap profile, the measurements taken were not precise enough at the postoperative stage, which raised the need for some approximations. Another limitation is the use of isotropic Ogden material model instead of relying on tissue microstructure that can enable the accurate representation of the tissue's anisotropic and regional variation of behaviour. However, while there is now sufficient information on the

collagen fibrils' distribution and anisotropy across corneal and scleral surface in healthy human eyes (148-150), the cross-thickness variation of fibril density is not yet well defined in the cornea. This point is of particular relevance to the current study where layers of corneal tissue are either separated or ablated, and hence assuming incorrectly a uniform cross-thickness fibril distribution may introduce significant errors in the model predictions.

In this study, for the first time it was possible to evaluate the importance of corneal material properties as a risk factor for the post-LASIK ectasia. It was done by means of numerical simulations. The future perspective of this finding is to integrate this concept with devices that are able to measure the corneal biomechanics *in vivo* and make it available for use by clinicians when screening patients for the risk of post-LASIK ectasia development.

5.4 Concluding remarks

This thesis aimed to evaluate the corneal material stiffness as a risk factor for post-LASIK ectasia. Patient-specific numerical models were built with different corneal stiffness according to previously described material constants. The corneal curvature of the numerical model was compared to the corresponding clinical curvature in order to establish the patient's material stiffness. We observed through this process that patients that developed the complication had softer corneas compared to those that remained stable. To the best of our knowledge, this was the first study to evaluate the material properties systematically in order to confirm the theory that stiffness could be a risk factor for the complication. This finding has clinical relevance since it is now possible to evaluate *in vivo* the corneal material properties on the preoperative screening of the patients and use this information for a better indication of the procedure.

References

1. Gehring WJ. The evolution of vision. Wiley Interdiscip Rev Dev Biol. 2014;3(1):1-40.
2. Holden BA, Fricke TR, Wilson DA, Jong M, Naidoo KS, Sankaridurg P, et al. Global Prevalence of Myopia and High Myopia and Temporal Trends from 2000 through 2050. Ophthalmology. 2016;123(5):1036-42.
3. Bourne RRA, Flaxman SR, Braithwaite T, Cicinelli MV, Das A, Jonas JB, et al. Magnitude, temporal trends, and projections of the global prevalence of blindness and distance and near vision impairment: a systematic review and meta-analysis. Lancet Glob Health. 2017;5(9):e888-e97.
4. Holden BA, Tahhan N, Jong M, Wilson DA, Fricke TR, Bourne R, et al. Towards better estimates of uncorrected presbyopia. Bull World Health Organ. 2015;93(10):667.
5. Smith TS, Frick KD, Holden BA, Fricke TR, Naidoo KS. Potential lost productivity resulting from the global burden of uncorrected refractive error. Bull World Health Organ. 2009;87(6):431-7.
6. Bourne RR, Stevens GA, White RA, Smith JL, Flaxman SR, Price H, et al. Causes of vision loss worldwide, 1990-2010: a systematic analysis. Lancet Glob Health. 2013;1(6):e339-49.
7. Shams N, Mobaraki H, Kamali M, Jafarzadehpour E. Comparison of quality of life between myopic patients with spectacles and contact lenses, and patients who have undergone refractive surgery. J Curr Ophthalmol. 2015;27(1-2):32-6.
8. Price MO, Price DA, Bucci FA, Jr., Durrie DS, Bond WI, Price FW, Jr. Three-Year Longitudinal Survey Comparing Visual Satisfaction with LASIK and Contact Lenses. Ophthalmology. 2016;123(8):1659-66.
9. Rose K, Harper R, Tromans C, Waterman C, Goldberg D, Haggerty C, et al. Quality of life in myopia. Br J Ophthalmol. 2000;84(9):1031-4.
10. Solomon KD, Fernandez de Castro LE, Sandoval HP, Biber JM, Groat B, Neff KD, et al. LASIK world literature review: quality of life and patient satisfaction. Ophthalmology. 2009;116(4):691-701.
11. Barraquer JI. The history and evolution of keratomileusis. Int Ophthalmol Clin. 1996;36(4):1-7.
12. Trokel SL, Srinivasan R, Braren B. Excimer laser surgery of the cornea. Am J Ophthalmol. 1983;96(6):710-5.
13. Marshall J, Trokel S, Rothery S, Schubert H. An ultrastructural study of corneal incisions induced by an excimer laser at 193 nm. Ophthalmology. 1985;92(6):749-58.
14. Maldonado-Codina C, Morgan PB, Efron N. Thermal consequences of photorefractive keratectomy. Cornea. 2001;20(5):509-15.
15. Reinstein DZ, Carp GI, Lewis TA, Archer TJ, Gobbe M. Outcomes for Myopic LASIK With the MEL 90 excimer laser. J Refract Surg. 2015;31(5):316-21.
16. Goweida MB. Intraoperative review of different bubble types formed during pneumodissection (big-bubble) deep anterior lamellar keratoplasty. Cornea. 2015;34(6):621-4.
17. Lopes BT, Ramos IC, Salomao MQ, Guerra FP, Schallhorn SC, Schallhorn JM, et al. Enhanced tomographic assessment to detect corneal ectasia based on artificial intelligence. Am J Ophthalmol. 2018.
18. Roberts C. The cornea is not a piece of plastic. Journal of refractive surgery. 2000;16(4):407-13.
19. Alio JL, Muftuoglu O, Ortiz D, Perez-Santonja JJ, Artola A, Ayala MJ, et al. Ten-year follow-up of laser in situ keratomileusis for high myopia. Am J Ophthalmol. 2008;145(1):55-64.
20. Ikeda T, Shimizu K, Igarashi A, Kasahara S, Kamiya K. Twelve-Year Follow-Up of Laser In Situ Keratomileusis for Moderate to High Myopia. Biomed Res Int. 2017;2017:9391436.

21. Alio JL, Soria F, Abbouda A, Pena-Garcia P. Laser in situ keratomileusis for -6.00 to -18.00 diopters of myopia and up to -5.00 diopters of astigmatism: 15-year follow-up. J Cataract Refract Surg. 2015;41(1):33-40.
22. Dupps WJ, Jr., Wilson SE. Biomechanics and wound healing in the cornea. Experimental eye research. 2006;83(4):709-20.
23. Elsheikh A. Finite element modeling of corneal biomechanical behavior. J Refract Surg. 2010;26(4):289-300.
24. Bao F, Wang J, Cao S, Liao N, Shu B, Zhao Y, et al. Development and clinical verification of numerical simulation for laser in situ keratomileusis. J Mech Behav Biomed Mater. 2018;83:126-34.
25. Kolb H. Gross Anatomy of the Eye. In: Kolb H, Fernandez E, Nelson R, editors. Webvision: The Organization of the Retina and Visual System. Salt Lake City (UT)1995.
26. DelMonte DW, Kim T. Anatomy and physiology of the cornea. Journal of cataract and refractive surgery. 2011;37(3):588-98.
27. Olver JM. Functional anatomy of the choroidal circulation: methyl methacrylate casting of human choroid. Eye (Lond). 1990;4 (Pt 2):262-72.
28. Hammond BR, Jr., Fuld K, Snodderly DM. Iris color and macular pigment optical density. Exp Eye Res. 1996;62(3):293-7.
29. Heavner W, Pevny L. Eye development and retinogenesis. Cold Spring Harb Perspect Biol. 2012;4(12).
30. Toris CB, Yablonski ME, Wang YL, Camras CB. Aqueous humor dynamics in the aging human eye. Am J Ophthalmol. 1999;127(4):407-12.
31. Goel M, Picciani RG, Lee RK, Bhattacharya SK. Aqueous humor dynamics: a review. Open Ophthalmol J. 2010;4:52-9.
32. Caprioli J, Coleman AL. Intraocular pressure fluctuation a risk factor for visual field progression at low intraocular pressures in the advanced glaucoma intervention study. Ophthalmology. 2008;115(7):1123-9 e3.
33. Schipper I, Senn P, Thomann U, Suppiger M. Intraocular pressure after excimer laser photorefractive keratectomy for myopia. J Refract Surg. 1995;11(5):366-70.
34. Chatterjee A, Shah S, Bessant DA, Naroo SA, Doyle SJ. Reduction in intraocular pressure after excimer laser photorefractive keratectomy. Correlation with pretreatment myopia. Ophthalmology. 1997;104(3):355-9.
35. Shah S, Chatterjee A, Mathai M, Kelly SP, Kwartz J, Henson D, et al. Relationship between corneal thickness and measured intraocular pressure in a general ophthalmology clinic. Ophthalmology. 1999;106(11):2154-60.
36. Bito LZ. The physiology and pathophysiology of intraocular fluids. Exp Eye Res. 1977;25 Suppl:273-89.
37. Kuszak JR. The ultrastructure of epithelial and fiber cells in the crystalline lens. International review of cytology. 1995;163:305-50.
38. Sakabe I, Oshika T, Lim SJ, Apple DJ. Anterior shift of zonular insertion onto the anterior surface of human crystalline lens with age. Ophthalmology. 1998;105(2):295-9.
39. Aliancy JF, Mamalis N. Crystalline Lens and Cataract. In: Kolb H, Fernandez E, Nelson R, editors. Webvision: The Organization of the Retina and Visual System. Salt Lake City (UT)1995.
40. Alio JL, Schimchak P, Negri HP, Montes-Mico R. Crystalline lens optical dysfunction through aging. Ophthalmology. 2005;112(11):2022-9.
41. Cook CA, Koretz JF, Pfahnl A, Hyun J, Kaufman PL. Aging of the human crystalline lens and anterior segment. Vision research. 1994;34(22):2945-54.
42. Amano S, Amano Y, Yamagami S, Miyai T, Miyata K, Samejima T, et al. Age-related changes in corneal and ocular higher-order wavefront aberrations. American journal of ophthalmology. 2004;137(6):988-92.
43. Muller LJ, Pels E, Vrensen GF. The specific architecture of the anterior stroma accounts for maintenance of corneal curvature. The British journal of ophthalmology. 2001;85(4):437-43.

44. Dua HS, Faraj LA, Said DG, Gray T, Lowe J. Human corneal anatomy redefined: a novel pre-Descemet's layer (Dua's layer). Ophthalmology. 2013;120(9):1778-85.
45. McKee HD, Irion LC, Carley FM, Brahma AK, Jafarinasab MR, Rahmati-Kamel M, et al. Re: Dua et al.: Human corneal anatomy redefined: a novel pre-Descemet layer (Dua's layer) (Ophthalmology 2013;120:1778-85). Ophthalmology. 2014;121(5):e24-5.
46. Dua HS, Faraj LA, Said DG, Gray T, Lowe J. Author reply: To PMID 23714320. Ophthalmology. 2014;121(5):e25-6.
47. Ehlers N, Heegaard S, Hjortdal J, Ivarsen A, Nielsen K, Prause JU. Morphological evaluation of normal human corneal epithelium. Acta Ophthalmol. 2010;88(8):858-61.
48. Reinstein DZ, Archer TJ, Gobbe M, Silverman RH, Coleman DJ. Epithelial thickness in the normal cornea: three-dimensional display with Artemis very high-frequency digital ultrasound. J Refract Surg. 2008;24(6):571-81.
49. Hanna C, Bicknell DS, O'Brien JE. Cell turnover in the adult human eye. Archives of ophthalmology. 1961;65:695-8.
50. Simon G, Ren Q, Kervick GN, Parel JM. Optics of the corneal epithelium. Refractive & corneal surgery. 1993;9(1):42-50.
51. Salomao MQ, Hofling-Lima AL, Lopes BT, Canedo ALC, Dawson DG, Carneiro-Freitas R, et al. Role of the corneal epithelium measurements in keratorefractive surgery. Curr Opin Ophthalmol. 2017;28(4):326-36.
52. Elsheikh A, Alhasso D, Rama P. Assessment of the epithelium's contribution to corneal biomechanics. Exp Eye Res. 2008;86(2):445-51.
53. Wilson SE, Hong JW. Bowman's layer structure and function: critical or dispensable to corneal function? A hypothesis. Cornea. 2000;19(4):417-20.
54. van Dijk K, Parker JS, Baydoun L, Ilyas A, Dapena I, Groeneveld-van Beek EA, et al. Bowman layer transplantation: 5-year results. Graefe's archive for clinical and experimental ophthalmology = Albrecht von Graefes Archiv fur klinische und experimentelle Ophthalmologie. 2018;256(6):1151-8.
55. Freegard TJ. The physical basis of transparency of the normal cornea. Eye. 1997;11 (Pt 4):465-71.
56. Meek KM, Knupp C. Corneal structure and transparency. Progress in retinal and eye research. 2015;49:1-16.
57. Liu X, Wang L, Ji J, Yao W, Wei W, Fan J, et al. A mechanical model of the cornea considering the crimping morphology of collagen fibrils. Investigative ophthalmology & visual science. 2014;55(4):2739-46.
58. Funderburgh JL, Mann MM, Funderburgh ML. Keratocyte phenotype mediates proteoglycan structure: a role for fibroblasts in corneal fibrosis. The Journal of biological chemistry. 2003;278(46):45629-37.
59. Jester JV, Moller-Pedersen T, Huang J, Sax CM, Kays WT, Cavangh HD, et al. The cellular basis of corneal transparency: evidence for 'corneal crystallins'. Journal of cell science. 1999;112 (Pt 5):613-22.
60. Kabosova A, Azar DT, Bannikov GA, Campbell KP, Durbeej M, Ghohestani RF, et al. Compositional differences between infant and adult human corneal basement membranes. Investigative ophthalmology & visual science. 2007;48(11):4989-99.
61. Puk O, Dalke C, Calzada-Wack J, Ahmad N, Klaften M, Wagner S, et al. Reduced corneal thickness and enlarged anterior chamber in a novel ColVIIIa2G257D mutant mouse. Investigative ophthalmology & visual science. 2009;50(12):5653-61.
62. Sridhar MS. Anatomy of cornea and ocular surface. Indian journal of ophthalmology. 2018;66(2):190-4.
63. Bonanno JA. Identity and regulation of ion transport mechanisms in the corneal endothelium. Progress in retinal and eye research. 2003;22(1):69-94.
64. Zavala J, Lopez Jaime GR, Rodriguez Barrientos CA, Valdez-Garcia J. Corneal endothelium: developmental strategies for regeneration. Eye. 2013;27(5):579-88.

65. Montes-Mico R, Cervino A, Ferrer-Blasco T, Garcia-Lazaro S, Madrid-Costa D. The tear film and the optical quality of the eye. Ocul Surf. 2010;8(4):185-92.
66. Escudero-Sanz I, Navarro R. Off-axis aberrations of a wide-angle schematic eye model. J Opt Soc Am A Opt Image Sci Vis. 1999;16(8):1881-91.
67. Espinosa J, Mas D, Kasprzak HT. Corneal primary aberrations compensation by oblique light incidence. Journal of biomedical optics. 2009;14(4):044003.
68. Liu T, Thibos LN. Compensation of corneal oblique astigmatism by internal optics: a theoretical analysis. Ophthalmic Physiol Opt. 2017;37(3):305-16.
69. Lu F, Wu J, Shen Y, Qu J, Wang Q, Xu C, et al. On the compensation of horizontal coma aberrations in young human eyes. Ophthalmic Physiol Opt. 2008;28(3):277-82.
70. Berrio E, Tabernero J, Artal P. Optical aberrations and alignment of the eye with age. Journal of vision. 2010;10(14).
71. Jones CE, Atchison DA, Meder R, Pope JM. Refractive index distribution and optical properties of the isolated human lens measured using magnetic resonance imaging (MRI). Vision Res. 2005;45(18):2352-66.
72. Fernandez J, Rodriguez-Vallejo M, Martinez J, Tauste A, Pinero DP. From Presbyopia to Cataracts: A Critical Review on Dysfunctional Lens Syndrome. J Ophthalmol. 2018;2018:4318405.
73. Westheimer G. Image quality in the human eye. Opt Acta (Lond). 1970;17(9):641-58.
74. Donnelly WJ, 3rd, Roorda A. Optimal pupil size in the human eye for axial resolution. J Opt Soc Am A Opt Image Sci Vis. 2003;20(11):2010-5.
75. d'Alessandro P. Retinal curvature and geometry of image formation. Brain Res. 2008;1225:67-75.
76. Artal P, Benito A, Tabernero J. The human eye is an example of robust optical design. J Vis. 2006;6(1):1-7.
77. Levy Y, Segal O, Avni I, Zadok D. Ocular higher-order aberrations in eyes with supernormal vision. Am J Ophthalmol. 2005;139(2):225-8.
78. Manche E, Roe J. Recent advances in wavefront-guided LASIK. Curr Opin Ophthalmol. 2018;29(4):286-91.
79. Pallikaris IG, Papatzanaki ME, Stathi EZ, Frenschock O, Georgiadis A. Laser in situ keratomileusis. Lasers Surg Med. 1990;10(5):463-8.
80. Ambrosio R, Jr., Wilson S. LASIK vs LASEK vs PRK: advantages and indications. Seminars in ophthalmology. 2003;18(1):2-10.
81. Shetty R, Francis M, Shroff R, Pahuja N, Khamar P, Girrish M, et al. Corneal Biomechanical Changes and Tissue Remodeling After SMILE and LASIK. Investigative ophthalmology & visual science. 2017;58(13):5703-12.
82. Osman IM, Helaly HA, Abdalla M, Shousha MA. Corneal biomechanical changes in eyes with small incision lenticule extraction and laser assisted in situ keratomileusis. BMC Ophthalmol. 2016;16:123.
83. Gatinel D, Chaabouni S, Adam PA, Munck J, Puech M, Hoang-Xuan T. Corneal hysteresis, resistance factor, topography, and pachymetry after corneal lamellar flap. J Refract Surg. 2007;23(1):76-84.
84. Leccisotti A, Fields SV, Moore J, Shah S, Moore TC. Changes in ocular biomechanics after femtosecond laser creation of a laser in situ keratomileusis flap. J Cataract Refract Surg. 2016;42(1):127-31.
85. Knox Cartwright NE, Tyrer JR, Jaycock PD, Marshall J. Effects of variation in depth and side cut angulations in LASIK and thin-flap LASIK using a femtosecond laser: a biomechanical study. J Refract Surg. 2012;28(6):419-25.
86. Seiler T, Koufala K, Richter G. Iatrogenic keratectasia after laser in situ keratomileusis. J Refract Surg. 1998;14(3):312-7.
87. Seiler T, Quurke AW. Iatrogenic keratectasia after LASIK in a case of forme fruste keratoconus. J Cataract Refract Surg. 1998;24(7):1007-9.

88. Naroo SA, Charman WN. Changes in posterior corneal curvature after photorefractive keratectomy. J Cataract Refract Surg. 2000;26(6):872-8.
89. Kamiya K, Oshika T, Amano S, Takahashi T, Tokunaga T, Miyata K. Influence of excimer laser photorefractive keratectomy on the posterior corneal surface. J Cataract Refract Surg. 2000;26(6):867-71.
90. Pallikaris IG, Kymionis GD, Astyrakakis NI. Corneal ectasia induced by laser in situ keratomileusis. Journal of cataract and refractive surgery. 2001;27(11):1796-802.
91. Randleman JB, Trattler WB, Stulting RD. Validation of the Ectasia Risk Score System for preoperative laser in situ keratomileusis screening. Am J Ophthalmol. 2008;145(5):813-8.
92. Santhiago MR, Smadja D, Wilson SE, Krueger RR, Monteiro ML, Randleman JB. Role of percent tissue altered on ectasia after LASIK in eyes with suspicious topography. J Refract Surg. 2015;31(4):258-65.
93. Chayet AS, Assil KK, Montes M, Espinosa-Lagana M, Castellanos A, Tsioulias G. Regression and its mechanisms after laser in situ keratomileusis in moderate and high myopia. Ophthalmology. 1998;105(7):1194-9.
94. Uchio E, Ohno S, Kudoh J, Aoki K, Kisielewicz LT. Simulation model of an eyeball based on finite element analysis on a supercomputer. British Journal of Ophthalmology. 1999;83(10):1106-11.
95. Chang HC, Hsu MY, Hsiao WT, Shum PJT. Finite Element Modeling of an Elderly Person's Cornea and Rigid Gas Permeable Contact Lenses for Presbyopic Patients. Appl Sci-Basel. 2018;8(6).
96. Remon L, Siedlecki D, Cabeza-Gil I, Calvo B. Influence of material and haptic design on the mechanical stability of intraocular lenses by means of finite-element modeling. J Biomed Opt. 2018;23(3).
97. Deenadayalu C, Mobasher B, Rajan SD, Hall GW. Refractive change induced by the LASIK flap in a biomechanical finite element model. Journal of Refractive Surgery. 2006;22(3):286-92.
98. Roy AS, Dupps WJ. Effects of Altered Corneal Stiffness on Native and Postoperative LASIK Corneal Biomechanical Behavior: A Whole-eye Finite Element Analysis. Journal of Refractive Surgery. 2009;25(10):875-87.
99. Roy AS, Dupps WJ. Patient-Specific Modeling of Corneal Refractive Surgery Outcomes and Inverse Estimation of Elastic Property Changes. J Biomech Eng-T Asme. 2011;133(1).
100. Roy AS, Dupps WJ, Roberts CJ. Comparison of biomechanical effects of small-incision lenticule extraction and laser in situ keratomileusis: Finite-element analysis. J Cataract Refr Surg. 2014;40(6):971-80.
101. Seven I, Vahdati A, Pedersen IB, Vestergaard A, Hjortdal J, Roberts CJ, et al. Contralateral Eye Comparison of SMILE and Flap-Based Corneal Refractive Surgery: Computational Analysis of Biomechanical Impact. Journal of Refractive Surgery. 2017;33(7):444-+.
102. Elsheikh A, Geraghty B, Alhasso D, Knappett J, Campanelli M, Rama P. Regional variation in the biomechanical properties of the human sclera. Experimental Eye Research. 2010;90(5):624-33.
103. Elsheikh A, Geraghty B, Rama P, Campanelli M, Meek KM. Characterization of age- related variation in corneal biomechanical properties. Journal of the Royal Society Interface. 2010;7(51):1475-85.
104. Whitford C, Studer H, Boote C, Meek KM, Elsheikh A. Biomechanical model of the human cornea: Considering shear stiffness and regional variation of collagen anisotropy and density. J Mech Behav Biomed. 2015;42:76-87.
105. Wang J. Numerical simulation of corneal refractive surgery based on improved reconstruction of corneal surface [PhD]: University of Liverpool; 2016.
106. Munnerlyn CR, Koons SJ, Marshall J. Photorefractive keratectomy: a technique for laser refractive surgery. J Cataract Refract Surg. 1988;14(1):46-52.
107. Chang AW, Tsang AC, Contreras JE, Huynh PD, Calvano CJ, Crnic-Rein TC, et al. Corneal tissue ablation depth and the Munnerlyn formula. J Cataract Refract Surg. 2003;29(6):1204-10.

108. Gatinel D, Saad A, Binder PS. Comparison of the effect of LASIK parameters on the percent tissue altered (1-dimensional metric) versus percent volume altered (3-dimensional metric). J Cataract Refract Surg. 2018;44(7):897-904.
109. Ogden RW. Non-linear Elastic Deformations: Dover Publications; 1997.
110. Eliasy A, Chen KJ, Vinciguerra R, Lopes BT, Abass A, Vinciguerra P, et al. Determination of Corneal Biomechanical Behavior in-vivo for Healthy Eyes Using CorVis ST Tonometry: Stress-Strain Index. Front Bioeng Biotechnol. 2019;7:105.
111. Pandolfi A, Manganiello F. A model for the human cornea: constitutive formulation and numerical analysis. Biomech Model Mechanobiol. 2006;5(4):237-46.
112. Elsheikh A, Whitford C, Hamarashid R, Kassem W, Joda A, Buchler P. Stress free configuration of the human eye. Med Eng Phys. 2013;35(2):211-6.
113. Patel S, Tutchenko L. The refractive index of the human cornea: A review. Cont Lens Anterior Eye. 2019.
114. Goodman S. A dirty dozen: twelve p-value misconceptions. Semin Hematol. 2008;45(3):135-40.
115. Belin MW, Khachikian SS. An introduction to understanding elevation-based topography: how elevation data are displayed - a review. Clin Exp Ophthalmol. 2009;37(1):14-29.
116. Cavas-Martinez F, De la Cruz Sanchez E, Nieto Martinez J, Fernandez Canavate FJ, Fernandez-Pacheco DG. Corneal topography in keratoconus: state of the art. Eye Vis (Lond). 2016;3:5.
117. Read SA, Collins MJ, Carney LG, Franklin RJ. The topography of the central and peripheral cornea. Invest Ophthalmol Vis Sci. 2006;47(4):1404-15.
118. Wang Z, Chen J, Yang B. Posterior corneal surface topographic changes after laser in situ keratomileusis are related to residual corneal bed thickness. Ophthalmology. 1999;106(2):406-9; discussion 9-10.
119. Seitz B, Torres F, Langenbucher A, Behrens A, Suarez E. Posterior corneal curvature changes after myopic laser in situ keratomileusis. Ophthalmology. 2001;108(4):666-72; discussion 73.
120. Baek T, Lee K, Kagaya F, Tomidokoro A, Amano S, Oshika T. Factors affecting the forward shift of posterior corneal surface after laser in situ keratomileusis. Ophthalmology. 2001;108(2):317-20.
121. Chan TC, Liu D, Yu M, Jhanji V. Longitudinal evaluation of posterior corneal elevation after laser refractive surgery using swept-source optical coherence tomography. Ophthalmology. 2015;122(4):687-92.
122. Ciolino JB, Belin MW. Changes in the posterior cornea after laser in situ keratomileusis and photorefractive keratectomy. J Cataract Refract Surg. 2006;32(9):1426-31.
123. Hashemi H, Mehravaran S. Corneal changes after laser refractive surgery for myopia: comparison of Orbscan II and Pentacam findings. J Cataract Refract Surg. 2007;33(5):841-7.
124. Randleman JB, Woodward M, Lynn MJ, Stulting RD. Risk assessment for ectasia after corneal refractive surgery. Ophthalmology. 2008;115(1):37-50.
125. Bohac M, Koncarevic M, Pasalic A, Biscevic A, Merlak M, Gabric N, et al. Incidence and Clinical Characteristics of Post LASIK Ectasia: A Review of over 30,000 LASIK Cases. Semin Ophthalmol. 2018;33(7-8):869-77.
126. Dawson DG, Randleman JB, Grossniklaus HE, O'Brien TP, Dubovy SR, Schmack I, et al. Corneal ectasia after excimer laser keratorefractive surgery: histopathology, ultrastructure, and pathophysiology. Ophthalmology. 2008;115(12):2181-91 e1.
127. Padmanabhan P, Aiswaryah R, Abinaya Priya V. Post-LASIK keratectasia triggered by eye rubbing and treated with topography-guided ablation and collagen cross-linking--a case report. Cornea. 2012;31(5):575-80.
128. Randleman JB, Russell B, Ward MA, Thompson KP, Stulting RD. Risk factors and prognosis for corneal ectasia after LASIK. Ophthalmology. 2003;110(2):267-75.
129. Santhiago MR, Giacomin NT, Smadja D, Bechara SJ. Ectasia risk factors in refractive surgery. Clin Ophthalmol. 2016;10:713-20.

130. Moshirfar M, Smedley JG, Muthappan V, Jarsted A, Ostler EM. Rate of ectasia and incidence of irregular topography in patients with unidentified preoperative risk factors undergoing femtosecond laser-assisted LASIK. Clin Ophthalmol. 2014;8:35-42.
131. Said A, Hamade IH, Tabbara KF. Late onset corneal ectasia after LASIK surgery. Saudi J Ophthalmol. 2011;25(3):225-30.
132. Buhren J, Schaffeler T, Kohnen T. Preoperative topographic characteristics of eyes that developed postoperative LASIK keratectasia. J Refract Surg. 2013;29(8):540-9.
133. Fernandez-Vega-Cueto L, Romano V, Zaldivar R, Gordillo CH, Aiello F, Madrid-Costa D, et al. Surgical Options for the Refractive Correction of Keratoconus: Myth or Reality. J Ophthalmol. 2017;2017:7589816.
134. Luce DA. Determining in vivo biomechanical properties of the cornea with an ocular response analyzer. J Cataract Refract Surg. 2005;31(1):156-62.
135. Hon Y, Lam AK. Corneal deformation measurement using Scheimpflug noncontact tonometry. Optom Vis Sci. 2013;90(1):e1-8.
136. Ortiz D, Pinero D, Shabayek MH, Arnalich-Montiel F, Alio JL. Corneal biomechanical properties in normal, post-laser in situ keratomileusis, and keratoconic eyes. J Cataract Refract Surg. 2007;33(8):1371-5.
137. Fontes BM, Ambrosio R, Jr., Jardim D, Velarde GC, Nose W. Corneal biomechanical metrics and anterior segment parameters in mild keratoconus. Ophthalmology. 2010;117(4):673-9.
138. Luz A, Lopes B, Hallahan KM, Valbon B, Ramos I, Faria-Correia F, et al. Enhanced Combined Tomography and Biomechanics Data for Distinguishing Forme Fruste Keratoconus. J Refract Surg. 2016;32(7):479-94.
139. Ambrósio R, Faria-Correia F, Ramos I, Valbon BF, Lopes B, Jardim D, et al. Enhanced Screening for Ectasia Susceptibility Among Refractive Candidates: The Role of Corneal Tomography and Biomechanics. Current Ophthalmology Reports. 2013;1(1):28-38.
140. Ambrósio Jr R, Ramos I, Luz A, Faria FC, Steinmueller A, Krug M, et al. Dynamic ultra high speed Scheimpflug imaging for assessing corneal biomechanical properties. Revista Brasileira de Oftalmologia. 2013;72:99-102.
141. Vinciguerra R, Ambrosio R, Jr., Elsheikh A, Roberts CJ, Lopes B, Morenghi E, et al. Detection of Keratoconus With a New Biomechanical Index. J Refract Surg. 2016;32(12):803-10.
142. Ambrosio R, Jr., Lopes BT, Faria-Correia F, Salomao MQ, Buhren J, Roberts CJ, et al. Integration of Scheimpflug-Based Corneal Tomography and Biomechanical Assessments for Enhancing Ectasia Detection. J Refract Surg. 2017;33(7):434-43.
143. Ferreira-Mendes J, Lopes BT, Faria-Correia F, Salomao MQ, Rodrigues-Barros S, Ambrosio R, Jr. Enhanced Ectasia Detection Using Corneal Tomography and Biomechanics. Am J Ophthalmol. 2019;197:7-16.
144. Vinciguerra R, Elsheikh A, Roberts CJ, Ambrosio R, Jr., Kang DS, Lopes BT, et al. Influence of Pachymetry and Intraocular Pressure on Dynamic Corneal Response Parameters in Healthy Patients. J Refract Surg. 2016;32(8):550-61.
145. Ambrosio R, Jr., Randleman JB. Screening for ectasia risk: what are we screening for and how should we screen for it? J Refract Surg. 2013;29(4):230-2.
146. Vinciguerra R, Ambrosio R, Jr., Roberts CJ, Azzolini C, Vinciguerra P. Biomechanical Characterization of Subclinical Keratoconus Without Topographic or Tomographic Abnormalities. J Refract Surg. 2017;33(6):399-407.
147. Klyce SD. Chasing the suspect: keratoconus. Br J Ophthalmol. 2009;93(7):845-7.
148. Aghamohammadzadeh H, Newton RH, Meek KM. X-ray scattering used to map the preferred collagen orientation in the human cornea and limbus. Structure. 2004;12(2):249-56.
149. Zhou D, Abass A, Eliasy A, Studer HP, Movchan A, Movchan N, et al. Microstructure-based numerical simulation of the mechanical behaviour of ocular tissue. J R Soc Interface. 2019;16(154):20180685.

150. Zhou D, Eliasy A, Abass A, Markov P, Whitford C, Boote C, et al. Analysis of X-ray scattering microstructure data for implementation in numerical simulations of ocular biomechanical behaviour. PLoS One. 2019;14(4):e0214770.

Appendix A. Ethical Approval Letter

温州医科大学附属眼视光医院医学伦理证明

项目名称： 角膜力学行为对 LASIK 术后角膜形态和屈光力的影响规律研究

项目负责人： 王勤美

项目承担单位： 温州医科大学

伦理委员会审查资料：

■实验方案（版本日期 2017.02.21 版本号 1.0） ■知情同意书（版本日期2017.02.21 版本号1.0） ■课题申报相关材料(版本日期2017.02.21 版本号 1.0)

涉及人的生物医学研究内容及研究方案摘要：

研究内容：

本项目拟创建在体测量角膜生物力学性能的方法，研发经个性化在体角膜生物力学性能矫正的 LASIK 手术的有限元数字预测模型，揭示角膜力学行为影响 LASIK 矫治效果的作用机理，为术式改进、手术设备研发等方面提供新途径。

研究内容：

1. 本项目拟纳入接受 LASIK 的近视患者 112 例。纳入标准：年龄 18~45 周岁；等效球镜度数-3.0~-6.0D，角膜散光小于 2D；符合 LASIK 手术适应症；保证术后 3 月都能回来随访；软镜停戴 2 周，硬镜停戴 4 周；理解和愿意配合此研究并签署知情同意书。

2. 检查流程：视觉和眼科检查，屈光不正度数(综合验光仪)，角膜地形图检查，眼球轴向数据和眼压(DCT)检查。术前、术后 1 周、1 月和 3 月随访。

伦理委员会审查意见：

同意申报

伦理委员会主任签名：

2017年 2月27 日

本伦理证明仅生于课题申报，有效期九个月。

Appendix B. Patient's Informed Consent Form

实验知情同意书

（版本日期：2014年02月20日，版本号1.0）

项目名称：LASIK个性化有限元预测模型的创建

研究者：王勤美

您被邀请参加这项研究是因为您具备参加该项研究的入组条件。请仔细阅读本知情同意书并慎重做出是否参加研究的决定。当您的研究医生或者研究人员和您讨论知情同意书的时候，您可以让他/她给您解释您看不明白的地方。我们鼓励您在做出参与此项研究的决定之前，和您的家人及朋友进行充分讨论。本研究的内容/性质、风险、不便或不适及其他重要信息如下：

若您正在参加别的研究，请告知您的研究医生或者研究人员。

王勤美医师将开展这项由温州医科大学附属视光医院资助的研究，本研究的资助者为温州医科大学附属视光医院。

1. 研究目的及背景、意义：

本研究的研究背景是近视已成为严重的公共卫生问题，准分子激光原位角膜磨镶术(LASIK)是矫正近视的最常见术式，但并不完美。高达7%的患者实际与预期近视矫正屈光度的差异超过±1.0D，手术精度有待提高。

本研究的研究目的是创建在体测量区域性角膜本构参量的方法，建立更好地预测手术矫治近视效果的LASIK个性化有限元预测模型；揭示角膜力学行为影响LASIK术后角膜形态及屈光力的作用机理，为术式改进和手术设备研发等方面提供参考。

2. 多少人将参与这项研究？

大约150人将参与在温州医学院附属眼视光医院进行的本研究。

3.本研究包括哪些内容？

如果您同意参加本研究，请您签署这份知情同意书。您将在术前、术后1周、1月、3月及6月总共接受5次检查，您将接受以下检查和程序以进一步确认您是否适合参加本研究：

①术前检查(Pre-operative measurements)

常规眼科检查

屈光不正度数(电脑验光仪、综合验光仪)

角膜曲率

角膜高度及厚度地形图(Pentacam测量3次)

全层角膜厚度(OCT)

接触式角膜厚度、眼轴长度、前房深度、晶状体厚度及玻璃体腔长度(A超)

眼压(ORA及DCT)

角膜生物力学性能测量(Corvis ST)

②术后检查(Post-operative measurements)

常规眼科检查

屈光不正度数(电脑验光仪、综合验光仪)

角膜曲率

角膜高度及厚度地形图(Pentacam测量3次)

角膜瓣厚度(OCT)

眼压(ORA及DCT)

角膜生物力学性能测量(Corvis ST)

4.这项研究会持续多久？

这项研究每次检查只要持续3个小时左右。您可以在任何时间选择退出研究而不受到任何惩罚，也不会丧失您本应获得的任何利益。然而，如果在研究途中您决定退出本研究，我们鼓励您先和您的医生商议。考虑到您的安全性问题，有可能在退出后，会进行一次相关检查。

5. 参加本研究的风险是什么？

本研究所涉及的所有检查均为当前临床常规使用且技术成熟的检查项目，安全性早已通过临床验证。但是也许在参与实验过程中您会感觉到眼部不适，我们将仔细评估您的眼部情况并给与相应的处理。我们会密切观察实验过程中每个受试者的情况，同时也请您将实验之前和之后感觉到的不适及时通知我们。本研究不会带来生理风险。我们会保证您信息的绝对安全，您的个人信息不会被泄露。研究过程中您随时都可以休息。

6. 参加研究的收益

如果您同意参加本研究，您将会得到您眼部详细的生物参数，这些信息有助于您更了解您眼睛的健康情况。很抱歉，由于我们经费有限，只能提供壹佰元人民币的经济补偿以表示您对我们研究工作的支持。若您中途退出研究时，也可得到最多为伍拾元人民币的相应的补偿。

7. 信息保密：

我们会按照法律的要求为您的研究记录保密。我国的相关法律为隐私、数据和授权访问的安全提供了保障。除非应相关法律要求，研究记录中您的姓名、身份证号码、地址、电话、或者任何可以直接辨别您身份的信息不会被泄露到温州医科大学附属眼视光医院之外。对那些传送到温州温州医科大学附属眼视光医院之外的关于您的研究信息，我们会用一个独一无二的编号代表您。编码信息将被妥善存放在温州医科大学附属眼视光医院。研究结果将永久保存在您的研究记录里。在科学会议或者科学杂志上发表本研究获得的研究信息和数据时，您的身份将不会被公开。

8.研究费用：

本研究所需要的全部费用（验光、角膜地形图、眼压计头、酬金等）由温州医科大学附属眼视光医院负责支付。

9. 参加研究的补偿：

很抱歉，由于我们经费有限，只能提供壹佰元人民币的经济补偿以表示您对我们研究工作的支持。若您中途退出研究时，也可得到最多为伍拾元人民币的相应的补偿。

10. 研究的风险

假如由于您参加本研究而导致损伤，温州医科大学附属眼视光医院会立刻提供必要的免费医疗护理，费用由温州医科大学附属眼视光医院支付。请在工作日联系王勤美医生，电话0577-88068880，在下班时间、周末或者节假日请通过联系包芳军0577-88067937，13388525505。**11. 拒绝参加或者退出研究的权利**

您参加试验是自愿的，可以拒绝参加或者有权在试验的任何阶段随时退出试验而不会遭到歧视或报复，其医疗待遇与权益不受影响。受试者中途退出后，今后将不收集与其有关的新数据。原则上，在您退出之后，研究者将严密保存您的相关信息直至销毁，期间不会继续使用或透露这些信息。

12. 如果您有问题或困难，该与谁联系？

如果您有与本研究相关的任何问题，请在工作日联系王勤美医生，电话0577-88068880，在下班时间、周末或者节假日请通过联系包芳军0577-88067937，13388525505。

如果您有与自身权利相关的任何问题，或者您想反映参与本研究过程中遭遇的困难、不满和忧虑，或者想提供与本研究有关的意见和建议，请联系温州医科大学附属眼视光医院医学伦理审查委员会，联系电话：0577-88053521，电子邮件：ysglunli@163.com.

告知声明

我已告知该受试者参加“LASIK个性化有限元预测模型的创建”的研究背景、目的、步骤、风险及获益情况，给予他/她足够的时间阅读知情同意书、与他人讨论，并解答了其有关研究的问题；我已告知该受试者当遇到与研究相关的问题时可随时与陈峰医生联系，遇到与自身权利/权益相关问题时随时与温州医学院附属眼视光医院医学伦理审查委员会联系，并提供了准确的联系方式；我已告知该受试者他/她可以退出本研究。我已告知该受试者他/她将得到这份知情同意书的副本，上面包含我和他/她的签名。

获得知情同意的研究人员签名　　日期

知情同意声明

我已被告知“LASIK个性化有限元预测模型的创建”的研究的背景、目的、步骤、风险及获益情况。我有足够的时间和机会进行提问，问题的答复我很满意。我也被告知，当我有问题、想反映困难、顾虑、对研究的建议，或想进一步获得信息，或为研究提供帮助时，应当与谁联系。我已经阅读这份知情同意书，并且同意参加本研究。我知道我可以在研究期间的任何时候无需任何理由退出本研究。我被告知我将得到这份知情同意书的副本，上面包含我和研究者的签名。

受试者签名　　日期